

Author's Accepted Manuscript

Magnetic field modulated dust streams from Jupiter
in interplanetary space

Alberto Flandes, Harald Krüger, Douglas P. Hamilton,
Linda Spilker, J. Francisco Valdés-Galicia, Rogelio
Caballero

PII: S0032-0633(11)00173-5
DOI: doi:10.1016/j.pss.2011.05.014
Reference: PSS 3108

To appear in: *Planetary and Space Science*

Received date: 27 October 2010
Revised date: 24 May 2011
Accepted date: 25 May 2011

Cite this article as: Alberto Flandes, Harald Krüger, Douglas P. Hamilton, Linda Spilker, J. Francisco Valdés-Galicia and Rogelio Caballero, Magnetic field modulated dust streams from Jupiter in interplanetary space, *Planetary and Space Science*, doi:10.1016/j.pss.2011.05.014

This is a PDF file of an unedited manuscript that has been accepted for publication. As a service to our customers we are providing this early version of the manuscript. The manuscript will undergo copyediting, typesetting, and review of the resulting galley proof before it is published in its final citable form. Please note that during the production process errors may be discovered which could affect the content, and all legal disclaimers that apply to the journal pertain.



www.elsevier.com/locate/pss

1
2
3
4
5
6
7
8
9
10
11
12
13
14
15
16
17
18
19
20
21
22
23
24
25
26
27
28
29
30
31
32
33
34
35
36
37
38
39
40
41
42
43
44
45
46
47
48
49
50
51
52
53
54
55
56
57
58
59
60
61
62
63
64
65

Magnetic field modulated dust streams from Jupiter in Interplanetary space

Alberto Flandes

Ciencias Espaciales, Instituto de Geofísica, UNAM, México.

Harald Krüger

Max-Planck-Institut für Sonnensystemforschung, 37191 Katlenburg-Lindau, Germany

Max-Planck-Institut für Kernphysik, 69029 Heidelberg, Germany.

Douglas P. Hamilton

University of Maryland, College Park, MD20742-2421, USA.

J. Francisco Valdés-Galicia

Ciencias Espaciales, Instituto de Geofísica, UNAM, México.

Linda Spilker

Jet Propulsion Laboratory/ California Institute of Technology, Pasadena, USA.

Rogelio Caballero

Ciencias Espaciales, Instituto de Geofísica, UNAM, México.

Abstract

High speed *dust streams* emanating from near Jupiter were first discovered by the Ulysses spacecraft in 1992. Since then, the phenomenon has been re-observed by Galileo in 1995, Cassini in 2000, and Ulysses in 2004. The dust grains are expected to be charged to a potential of $\sim 5V$, which is sufficient to allow the planet's magnetic field to accelerate them away from the planet, where they are subsequently influenced by the interplanetary magnetic field (IMF). A similar phenomenon was observed near Saturn by Cassini. Here, we report and ana-

1
2
3
4
5
6
7
8
9 lyze simultaneous dust, IMF and solar wind data for all dust streams from the two
10 Ulysses Jupiter flybys. We find that compression regions (CRs) in the IMF - re-
11 gions of enhanced magnetic field - precede most dust streams. Furthermore, the
12 duration of a dust stream is roughly comparable with that of the precedent CR, and
13 the occurrence of a dust stream and the occurrence of the previous CR are sepa-
14 rated by a time interval that depends on the distance to Jupiter. The intensity of
15 the dust streams and their precedent CRs are also correlated, but this correlation is
16 only evident at distances from the planet no greater than $2 AU$. Combining these
17 observations, we argue that CRs strongly affect dust streams, probably by deflect-
18 ing dust grain trajectories, so that they can reach the spacecraft and be detected by
19 its dust sensor.
20
21
22
23
24
25
26
27
28
29

30 *Keywords:* Interplanetary Dust, Solar wind, Jupiter, Io
31
32
33
34
35
36
37
38
39
40
41
42
43
44
45
46
47
48
49
50
51
52
53
54
55
56
57
58
59
60
61
62
63
64
65

1. INTRODUCTION

The spectacular volcanic plumes of Jupiter's moon Io inject copious amounts of gas and fine dust along Io's orbit, leading to the so-called Io plasma torus at $\sim 5.9 R_J$ distance from Jupiter (Jupiter radius $R_J = 71,492$ km). Dust grains in Io's volcanic plumes get easily charged in Io's ionosphere (?) and transported into the plasma torus (Horányi et al., 1993). At least one kilogram of sub-micrometric (~ 10 nm) dust grains escape every second from the torus to the circum-jovian space (?). Due to their electric charge and small size, their motion is dominated by electromagnetic forces. It has been demonstrated that the induced corotating electric field of the huge jovian magnetic field accelerates positively charged grains away from Jupiter. The grains get sufficiently large speeds (≥ 200 km s⁻¹) that they can easily escape from the magnetosphere (??).

This escape was first observed by Ulysses in 1992 and confirmed by the Galileo (1995) and Cassini (2000) spacecraft which detected this dust outside the jovian magnetosphere as a discontinuous, but periodic flux coupled to the interplanetary magnetic field (IMF) (???). This phenomenon was called the jovian dust streams. The Cassini spacecraft detected dust streams escaping from the Saturn system as well in 2004 (?). It was shown that these two phenomena shared similar properties. The saturnian dust streams source is not well defined yet, however the cryovolcanic jets from the south pole of the moon Enceladus appear to be good candidates (?). Nevertheless, the saturnian charged dust grains also escape via the corotational electric field of Saturn mainly along the planet's equatorial plane (??). Recently ? explained the saturnian dust stream detection by Cassini CDA (Cosmic Dust Analyzer) in connection to the IMF and concluded that the saturnian dust streams particles were directly correlated to the sector structure of the

1
2
3
4
5
6
7
8
9
26 IMF, in particular the positive sectors.

11 In this work we concentrate on the jovian dust streams detected during the
12 two flybys of the Ulysses spacecraft at Jupiter (1991-1992 and 2003-2005). This
13 data set is, by far, the most complete and comprehensive presently available (?).
14 We present the full data set in a series of 13 plots (Fig. 1a to Fig. 1m) that will
15 be discussed throughout this work. Our intention is to give the reader a better
16 understanding of the detection and analysis of dust streams, and to elucidate the
17 close connection that they have with the IMF and the solar wind. We investigate
18 the significance of Corotating Interaction Regions (CIRs) and Coronal Mass Ejec-
19 tions (CMEs) for the formation of the jovian dust streams in interplanetary space.
20 A very first approach to this study was sketched in ?, nevertheless in this work we
21 present a more thorough and extensive analysis.
22
23
24
25
26
27
28
29
30
31
32

33 **2. THE ULYSSES TRAJECTORY AND THE JOVIAN DUST**

34
35
36
37
38
39 The Ulysses spacecraft was launched towards Jupiter in October 1990. In early
40 1992, during the first Jupiter flyby, a swing-by manoeuvre changed the inclination
41 of its orbit to 79° with respect to the ecliptic plane. Since then, Ulysses has been
42 on an eccentric heliocentric trajectory with an approximately six-year period and
43 5.4 AU aphelion distance. Ulysses is no longer active. After almost 19 years and
44 a very successful mission, the Ulysses spacecraft was switched off in June 2009.
45 Figure 2 shows the orbits of Jupiter and Ulysses about the Sun during the second
46 Jupiter flyby. The two Ulysses flybys differed in geometry as can be seen in the
47 top panels of Figure 3a and Fig. 3b that show the profiles of the Ulysses angular
48 position with respect to Jupiter.

49 During the first flyby, Ulysses approached Jupiter to $6.3 R_J$ moving close to

1
2
3
4
5
6
7
8
9
50 the ecliptic plane and close to the Jupiter-Sun line (Fig. 3a, top panel), i.e. at
11 low jovigraphic and ecliptic latitudes and low jovigraphic longitudes. After flyby,
12
13 52 Ulysses moved away from the planet at approximately -35° jovigraphic latitude.

14
15 53 During the first flyby, Ulysses scanned only a narrow region of circum-jovian
16 space, but its radial distance was very close to Jupiter ($6.3 R_J$). During the second
17 54 flyby, between 2002 and 2004 (Fig. 3b, bottom panel), the spacecraft scanned
18 55 a wider range of jovigraphic latitudes and longitudes: Ulysses sampled more
19 56 than 120° in longitude and more than 100° in latitude. During this second flyby,
20 57 Ulysses approached Jupiter to only 0.8 AU in early 2004.
21 58

27 2.1. *Dust stream detection and identification*

28
29 60 Ulysses detected the very first dust stream as a weak burst in late September
30 61 1991, at $r = 1.1$ AU distance from Jupiter while heading towards Jupiter along the
31 62 ecliptic plane at a jovigraphic longitude of $L \approx 11^\circ$. Jovigraphic longitudes are
32 63 defined with respect to the Sun-Jupiter-spacecraft angle. The Jupiter-Sun vector
33 64 defines $L = 0^\circ$. Positive longitudes correspond to angles to the left of that imag-
34 65 inary line (in the direction of Jupiter's motion) - see Fig.2. We also define the
35 66 jovigraphic latitude, β , as the angle measured with respect to the jovian equatorial
36 67 plane. Positive latitudes correspond to the northern hemisphere and negative lati-
37 68 tudes to the southern hemisphere. We ignore the small tilt of Jupiter's rotation axis
38 69 (1.31°) and that of the solar equator (6.09°) and assume that these are coplanar.

39
40
41
42
43
44
45
46
47 70 During this first flyby, eleven dust streams were detected, five before the clos-
48 71 est approach and six while the spacecraft was flying away from Jupiter. The last
49 72 dust stream of this flyby was detected on 19 October, 1992 about 2 AU away from
50 73 Jupiter. During the second flyby, the first dust stream was detected in November
51 74 2002 as a weak burst as well, but this time, when the spacecraft was at $r=3.4$ AU,

1
2
3
4
5
6
7
8
9
10 75 three times farther away from Jupiter as compared to the first dust stream from
11 76 the first flyby. Then the spacecraft was at a jovigraphic longitude and latitude
12
13 77 $L = -37^\circ$ and $\beta = 44^\circ$. Unfortunately, after the detection of this dust stream the
14
15 78 dust detector was switched off on 1st of December of 2002 for a six month pe-
16
17 79 riod for power saving reasons on board the spacecraft. Nevertheless many more
18
19 80 streams were observed when the detector was switched on again on 3 June 2003.
20
21 81 The data indicate that dust streams are detected fairly uniformly in a wide range
22
23 82 of jovigraphic latitudes and longitudes. In total, 28 dust streams were registered,
24
25 83 nine before the closest approach and nineteen while Ulysses was receding in ra-
26
27 84 dial distance from the planet. Actually the last dust stream was detected on 16
28
29 85 August, 2005 around 4 AU away from Jupiter (?).

30
31 86 The earliest dust stream identification was made by ? and the streams have
32
33 87 been a topic of intense study for over 15 years. In all cases, dust streams were
34
35 88 identified with probabilistic methods based on Poisson statistics (?). This method
36
37 89 separates true dust streams from chance random fluctuations in the dust impact
38
39 90 rate. In our work, we adopt the dust stream identifications and other relevant
40
41 91 parameters from ? and ?. The first work provides a description of the Ulysses first
42
43 92 flyby dust stream identification and the second work provides a comprehensive
44
45 93 up-to-date summary of all the Ulysses dust streams from the second flyby. We
46
47 94 keep the stream numbers and order after ? and ?, but for practical purposes, we
48
49 95 will designate the streams of the first flyby as streams 101 through 111 and those
50
51 96 of the second flyby as 201 through 228, where the first digit stands for the flyby
52
53 97 number and the last two for the dust stream number (See Table 1 and bottom panel
54
55 98 of Fig. 1a to Fig. 1m).

99 3. THE IMF, THE SOLAR WIND AND THE DUST STREAMS

100 ? suggested that dust streams could be connected to corotating interaction re-
101 gions (CIRs). ? proposed a model that explained the periodicity of dust streams
102 through the successive and alternate deflections of the dust trajectories by the peri-
103 odic change of polarity of the interplanetary magnetic field (IMF). In 2006, in the
104 dust stream data set from the second Jupiter flyby, ? found correlations between
105 the intensities of the radial (B_R) and tangential (B_T) magnetic field components
106 and some of the dust streams' properties as well as footprints of the solar rotation
107 period.

108 3.1. CIR and CME identification

109 The solar wind is a supersonic nearly radial outward flow of plasma that forms
110 the heliosphere. It results from the expansion of the outermost layer of the Sun,
111 the corona, and carries away the solar magnetic field, which is twisted due to the
112 rotation of the Sun. This leads to the structure known as the Archimedean spiral.

113 Observations (?) have established that coronal holes at the Sun are stable
114 sources of fast wind that lead to a pattern of corotating fast and slow solar wind
115 flows in the heliosphere. The increasing interaction between these two flows with
116 distance from the Sun generates the confined regions known as Corotating Inter-
117 action Regions, or CIRs, that evolve as corotating spirals in the solar equatorial
118 plane. CIRs are bound by a forward pressure wave as leading edge that propa-
119 gates into a slower moving plasma, and a reverse compression wave as trailing
120 edge propagating back into a faster plasma. In contrast, Coronal Mass Ejections,
121 or CMEs, are events where relatively dense and discretely bound coronal material
122 is propelled outwards from the Sun to the interplanetary space.

1
2
3
4
5
6
7
8
9
10 123 For our analysis we use IMF and solar wind data obtained from the Ulysses
11 124 spacecraft homepage (<http://ulysses.jpl.nasa.gov/>). The solar wind pa-
12 125 rameters (rows 1-3) are derived from the Swoops/Ion experiment (see ? for fur-
13 126 ther details). These instruments measured the vector of the IMF and the speeds
14 127 and densities of the solar wind plasma; while IMF parameters (rows 4 and 5 in
15 128 Fig. 1) are derived from the VHM/FGM experiment (Vector Helium Magnetome-
16 129 ter/Flux Gate Magnetometer experiment; we refer the reader to ?) for further
17 130 details.

18
19
20
21
22
23
24 131 For CIR and CME identification purposes, in Figures 1*a*–1*m*, we plot the main
25 132 properties of the solar wind and the IMF. These are the proton speed (V), number
26 133 density (N_p) and temperature (T_p), as well as the intensity of the magnetic field
27 134 vector B and the azimuthal angle of the magnetic field defined as Φ .

28
29
30
31
32 135 We assume that the proton species dominate the solar wind and their properties
33 136 reflect well those of the bulk solar wind. We also consider that the dynamics of
34 137 charged grains is mainly dominated by the tangential component of the magnetic
35 138 field vector (see Panel 4 of Fig. 1*a* - 1*m*). The latter assumption applies because
36 139 at Jupiter, the IMF vector roughly lies in the ecliptic plane and it is also roughly
37 140 perpendicular to the Jupiter-Sun line.

38
39
40
41
42
43 141 CIRs are a common and repetitive feature of the solar wind. They are bounded
44 142 by shocks which cause sharp changes to the solar wind speed V at both their
45 143 leading and trailing sides. A nice train of five CIRs associated with streams 212
46 144 to 216 can be seen in Fig. 1*i*, between days 150 and 203 in 2004 - note the sharp
47 145 vertical steps in V that bound the CIRs.

48
49
50
51
52
53 146 The first step is the fast forward shock produced when the fast solar wind
54 147 plasma reaches and collides with the leading slow solar wind plasma, and the sec-

1
2
3
4
5
6
7
8
9
10
11
12
13
14
15
16
17
18
19
20
21
22
23
24
25
26
27
28
29
30
31
32
33
34
35
36
37
38
39
40
41
42
43
44
45
46
47
48
49
50
51
52
53
54
55
56
57
58
59
60
61
62
63
64
65

148 ond step is the reverse shock produced when the rear fast wind tries to detach itself
149 from the trailing slow wind. Additionally, we see well defined enhancements in
150 B , T_p and N_p , all of which are expected when plasma is significantly compressed.

151 In summary, our method of CIR identification relies on the abrupt increase in
152 the solar wind speed at the beginning correlated with strong enhancements of the
153 magnetic field strength. The identification is confirmed with the simultaneous en-
154 hancement of the plasma number density and temperature. We state that whether
155 we may be using a computer algorithm to identify the IMF enhancements, a sec-
156 ond confirmation by direct inspection of the data, was always necessary.

157 Identification of CMEs follows slightly different rules. During a CME, we still
158 expect enhancements of the IMF strength and solar wind parameters N_p , V and
159 T_p . Although, the fastest and most evident CMEs show a leading shock (sharp
160 change in V), they do not have a rear bounding shock. Instead, the plasma speed
161 declines smoothly until it reaches average solar wind speed values. This is the
162 main distinguishing characteristic between CIRs and CMEs. Additional clues
163 come from the fact that CIRs are expected to occur, on average, twice per solar
164 rotation period (every two weeks) when the spacecraft crosses the Sun's current
165 sheet, while CMEs show no periodicity and are greatly outnumbered by the CIRs.
166 Finally, at Jupiter's distance CMEs are usually magnetically weak compared to
167 CIRs. CMEs connected to dust streams are not very obvious in Fig. 1, but one
168 intense example can be seen in Fig 1j around day 259 in 2004. A clear single step
169 in V is observed at the beginning of the event but there is no second step.

170 Both Ulysses flybys of Jupiter occurred shortly after solar maxima (1990-1991
171 and \sim 2001) so, in some cases, the solar wind appears quite perturbed. This
172 makes the identification of the solar wind structures especially complex, leading

1
2
3
4
5
6
7
8
9
10 173 to uncertainties in some cases. Despite these uncertainties, it is clear that most
11 174 of the 39 dust streams detected in both flybys are connected to CIRs rather than
12
13 175 CMEs. From Ulysses' first pass by Jupiter, at most three of eleven dust streams
14
15 176 (streams 105, 109 and 110) are likely related to CMEs. From the second flyby, five
16
17 177 streams seem linked to one of these events (201, 202, 203, 217 and 225). Some
18
19 178 identifications of solar wind events are uncertain. For example, it appears as if
20
21 179 stream 201 is correlated with a CME that occurred began on day 324 (or perhaps
22
23 180 326), but which has an unclearing time. In addition, the events prior streams
24
25 181 202 and 203 seem to combinations of both CIRs and CMEs (Table 1).

26
27 182 In Table 1, we summarize all events connected to dust streams and mark some
28
29 183 special cases with asterisks. Still, we highlight that our interest lies in the solar
30
31 184 wind magnetic field enhanced regions where plasma is compressed and leads to
32
33 185 a stronger deflection of interplanetary dust grains trajectories provided by either
34
35 186 CIRs or the leading regions of CMEs. For simplicity, we will usually refer to
36
37 187 either of these events simply as compression regions (CRs), bearing in mind that
38
39 188 in the majority of cases these are CIRs.

40
41 189 A direct comparison between the jovian dust streams and the IMF and solar
42
43 190 wind data from both Ulysses' Jupiter flybys (Fig. 1) shows that every dust stream
44
45 191 is preceded by at least one CR. This fact can easily be observed in figures 1a to
46
47 192 1m where every dust stream (bottom panel, numbered shaded rectangles) and its
48
49 193 associated compression regions (vertical dark grey stripes) are highlighted. Of
50
51 194 course with CIRs occurring on average every two weeks, there is always a CR
52
53 195 shortly (few days) before a dust stream, though sometimes at the same time. These
54
55 196 former CRs are precisely the ones that are highlighted with darker tones, since
56
57 197 they likely influence the dust streams. Our next task is to determine whether

1
2
3
4
5
6
7
8
9 198 these associations are random or have a direct cause and relationship with the dust
10 streams.
11

12
13 200 Notice that in Fig. 1 and for the time periods that we consider for our study
14 -when possible-, all CRs are highlighted with gray stripes. Darker stripes repre-
15 201 -sent the CRs that are likely associated to dust streams chosen as the immediate
16 202 preceding CR, either a CIR or a CME.
17
18 203

19
20 204 We introduce Fig. 4 as a complement of Fig.1, in order to have a better com-
21 parison of both flybys and to highlight some features that play an important role in
22 205 our analysis and that are discussed in the following sections. The top panel shows
23 the jovicentric detection distances of each stream during both flybys (+: first flyby
24 206 and Δ : second flyby). The middle panel shows the dust flux of each dust stream.
25 Note in this panel a *peak* (212-214) in the flux (2nd flyby) that corresponds to
26 207 the jovian equatorial plane crossing. The bottom panel shows the time separation
27 between each dust stream and its precedent compression region, which show a
28 208 variation with distance.
29
30 209
31
32 210
33 211
34 212
35
36
37
38

39 213 3.2. Dust stream durations

40
41 214 Figures 1a to 1m and Table 1 suggest that the duration of dust streams (Δt_s)
42 is well connected to the duration of the CRs (Δt_c). The average impact rate of
43 215 most interplanetary and interstellar particles detected by the dust detector in quiet
44 216 times is around one impact every 10 days. The dust stream flux can increase this
45 217 rate by one to four orders of magnitude. These enhancements define how long or
46 218 short dust streams are. We refer the reader to ? and ? for the dust stream duration
47 219 calculation details. The dust streams durations determined this way are listed in
48 220 Table 1, column 3 with accuracies of approximately ± 0.5 days.
49
50
51
52
53
54 221
55

56 222 For comparison purposes, we also calculate the durations of CIRs and/or CMEs.
57
58

1
2
3
4
5
6
7
8
9
223 Since CIRs are bounded by forward and reverse shocks it is somewhat easier to
10
224 get their durations more accurately. By contrast, the durations of CMEs, and in-
11
12 deed their identification, is more uncertain since these are bounded -in the most
13
225 evident cases- only by a fast forward shock. Nevertheless we only consider the
14
226 duration of the compression region that leads the CME, which in most cases can
15
16
17 227 duration of the compression region that leads the CME, which in most cases can
18
19 228 be inferred with the aid of the other properties of the solar wind -like density and
20
21 229 temperature- and the IMF.

22
23 230 Note that in some cases, complicated CRs are correlated with dust streams of
24
25 231 similar complex appearance. An excellent example is stream 211 which, although
26
27 232 classified as a single stream of 8.1 day duration in Table 1, has a double-peaked
28
29 233 structure and may in fact be two streams separated by few days (Fig. 1h, days 74-
30
31 234 84). Interestingly, two CIRs occur just prior to the two streams. As Ulysses was
32
33 235 about 30 degrees above the jovian equator at this point, strong positive forces (note
34
35 236 the F_n trace) were required to deflect grain trajectories upward; and indeed, strong
36
37 237 positive F_n values occur 1-2 days before each sub-stream. A more borderline
38
39 238 example is dust stream 205 (Fig.1g), which has a long duration but might also
40
41 239 possibly be better separated into two distinct streams. This stream follows two
42
43 240 chained CIRs between days 276.0 and 286.3. Clearly in most cases CIR and
44
45 241 stream identification is a bit subjective. For analysis purposes in this paper, we
46
47 242 consider all of these possible double events as long single events.

48
49 243 Also note that stream 211 and stream 205, with durations of around seven
50
51 244 days, are almost twice as long as the average stream duration. In fact, streams 212,
52
53 245 213 and 214 are even longer, showing durations of about 10 days (Fig. 1i). There
54
55 246 is not an obvious way to separate these streams into several smaller ones and,
56
57 247 conversely, a case can be made for combining streams 213 and 214 and perhaps

1
2
3
4
5
6
7
8
9
248 even 212 into one continuous and extremely long dust stream! Strong and regular
10
11 249 CIRs also occur during this time, but their durations do not correlate with the
12
13 250 durations of the dust streams. There is clearly another effect at work here. Most
14
15 251 likely, the fact that Ulysses was near the Jovian equator during this time period is
16
17 252 important, as dust trajectories do not need to be altered as much and, thus have
18
19 253 a higher chance to reach the dust sensor. This would naturally lead to a higher
20
21 254 flux. These long streams are, nevertheless, indicated for reference purposes in the
22
23 255 summary figures we will present below.

24
25 256 Figure 5 shows the direct comparison of the dust stream durations and the du-
26
27 257 rations of their previous CR. We have used the dust stream numbers as markers
28
29 258 to highlight the individual durations. Both, the durations of dust streams and their
30
31 259 precedent CRs are similar, typically around 4 days. Both flybys are analyzed sep-
32
33 260 arately as well considering that, in each case, the dust stream detection geometry
34
35 261 was different, which seems to make a difference as can be seen comparing Fig.5a
36
37 262 and Fig.5b. Even though the durations are well correlated, the correlation coef-
38
39 263 ficients confirm this dependence on geometry: The first flyby data show a better
40
41 264 correlation coefficient (0.80) than the second flyby (0.69). For our statistical pur-
42
43 265 poses, we note that streams 212, 213 and 214 were atypically long and we exclude
44
45 266 them from our correlation analysis. In the following sections we will also keep
46
47 267 this separate analysis of both flybys.

268 3.3. *CRs and dust stream non-simultaneous detection*

269
270 In section 3.1, we have shown that the dust streams appear shifted in time
271
272 with respect to the precedent high IMF event. It is also evident that the closer to
273
274 Jupiter, the closer in time also the occurrence of every dust stream with respect to
275
276 its previous event. Thus, this time delay between the detection of a CR and the

1
2
3
4
5
6
7
8
9
273 detection of the dust stream that follows varies with the distance from Ulysses to
10
274 Jupiter. For analysis purposes this offset is measured from the beginning of each
11
12
13 275 dust stream to the beginning of the precedent IMF event. This correlation is shown
14
15 276 in Fig.6. Figure 6a shows that the correlation coefficient in the first flyby data set
16
17 277 is 0.78. The second flyby data (Fig.6b) shows a weaker correlation coefficient
18
19 278 (0.54) in particular, due to the dust streams detected farther away from Jupiter.
20
21 279 Still, in a good number of cases, we can say that the delay between each stream
22
23 280 and its precedent CR grows with the jovicentric distance.

24
25 281 The travelled distance depends on the traveling speed of the grains through
26
27 282 interplanetary space and, in turn, this speed depends on the acceleration mecha-
28
29 283 nisms inside the jovian magnetosphere. This problem has been discussed by many
30
31 284 authors over the past 15 years (????). Considering that ? estimated grain veloc-
32
33 285 ities ($\geq 200 \text{ km s}^{-1}$) and that ? derived values between 300 and 400 km s^{-1} , we
34
35 286 adopt $v \sim 400 \text{ km s}^{-1}$ and we can say that dust grains traverse the jovian magneto-
36
37 287 sphere in about 3 hours and, afterwards, travel an AU in about 4 days. For all dust
38
39 288 streams, therefore, the dust travel time is well approximated by the interplanetary
40
41 289 portion of its trajectory, i.e. $t_S (\text{days}) \approx 4.3 r (\text{AU})$.

42 43 290 3.4. Dust stream intensities

44
45 291 The intensity of each dust stream seems to depend on the intensity of its prece-
46
47 292 dent CR, suggesting again that dust streams are, at least, modulated by the CRs.
48
49 293 In fact, intense (roughly $B \geq 2 \text{ nT}$) and/or long CRs lead to intense and/or long
50
51 294 dust streams, and weak CRs lead to weak streams or no stream at all. Weak CRs
52
53 295 likely produce dust streams only near the jovian magnetosphere and the jovian
54
55 296 equatorial plane where the dust population is larger. Examples of this can be
56
57 297 seen throughout the full data set as in Fig.1h, where a couple of weak CIRs (one,

1
2
3
4
5
6
7
8
9
298 $B \sim 1.4\text{nT}$, around day 10 in 2004 and the other, $B \sim 1.5\text{nT}$, around day 30, both
10
11 close to Jupiter, but with the spacecraft at high latitude ($\beta > 50^\circ$) do not produce
12
13 dust streams. However, there are some cases when no dust streams are detected
14
15 even after strong enough CRs. Take for example Fig 1a, between days 290 and
16
17 330 in 1991. Even though there is a faint hint of streams in the dust rate profile,
18
19 there are not enough dust impacts for a clear stream identification. A probable ex-
20
21 planation to this lies in the fact that the dust flux from Jupiter, though continuous,
22
23 is not steady at all. Two main factors are involved in this. One is the dust produc-
24
25 tion through Io's volcanism and the other is the plasma environment in Jupiter's
26
27 magnetosphere. The first one controls the dust supply into the plasma torus and
28
29 the magnetosphere; the other controls the dust charging and therefore the jovian
30
31 dust supply to the interplanetary medium. Nevertheless, a comparison between
32
33 the dust stream flux and their precedent CR's magnetic field intensity apparently
34
35 show contradictory results (see Fig.7). The first flyby data supports the former hy-
36
37 pothesis and shows a clear correlation ($R = 0.75$) between both sets. In contrast,
38
39 the second flyby data does not show an apparent correlation. Again distance and
40
314 geometry may explain this discrepancy.

315 **4. INTERACTION OF DUST STREAMS WITH THE IMF**

316 *4.1. Grain charge*

317 During the grains' journey away from Jupiter, their surface electric charge Q
318 is not strictly constant. In particular, inside the plasma torus, the different plasma
319 conditions modulate Q . Higher dusk side temperatures, result in dominance of
320 secondary electron emission currents over the other currents producing positively
321 charged dust grains, that will be able to escape from the jovian magnetosphere

1
2
3
4
5
6
7
8
9
322 (?) These grains have typical $\phi \approx +5$ volts surface potentials (equivalent to ≈ 35
323 fundamental charges if $a = 10$ nm). Outside of the magnetosphere, Q could be
324 affected essentially by the interaction with the solar wind ions and electrons and
325 the UV solar radiation. The effects of the UV photons on the dust stream grains
326 can be evaluated with:

$$I_v = 2.5 \times 10^{10} \pi a^2 e (\chi / r_{AU}^2) \exp(-e\phi / kT_v) \quad (1)$$

327 which approximates the production of photoelectrons due to solar UV radia-
328 tion from positively charged dust grains (?). Here χ is the efficiency factor whose
329 value can be taken as 0.1 for dielectric conductors such as silicates. If at $r_{AU} = 5.2$,
330 the UV photons' energy is of the order of $kT_v \approx 2$ eV, the electron current from
331 a 10 nm particle would be 0.001 electrons/day which is a very low rate for the
332 periods of time considered in our study. In general, collection currents from solar
333 wind ions and electrons are more efficient than UV photoemission currents.

334 Solar wind charging effects are more efficient than UV photons'. The solar
335 wind is mainly characterized by ions and electrons. Solar wind ions have an av-
336 erage energy of the order of 1 keV at the orbit of Jupiter and electrons around
337 1 eV, nevertheless the dust stream grains have velocities that are comparable to
338 the solar wind particles, therefore, in some cases, collisions may involve larger
339 energies. On average, the grain net charging will depend on the initial sign of its
340 charge, its relative velocity with respect to the ions/electrons and the encounter
341 frequency between grains and solar wind particles. This frequency of encounters
342 may tell us how relevant these encounters are for charging purposes. Let us define
343 this rate as $T = v\lambda^{-1}$ with v as the velocity of the dust grains with respect to the
344 solar wind and λ the mean free path, which is defined in terms of the solar wind

1
2
3
4
5
6
7
8
9
10
11
12
13
14
15
16
17
18
19
20
21
22
23
24
25
26
27
28
29
30
31
32
33
34
35
36
37
38
39
40
41
42
43
44
45
46
47
48
49
50
51
52
53
54
55
56
57
58
59
60
61
62
63
64
65

1
2
3
4
5
6
7
8
9
345 ion/electron density n and σ the capture cross sectional area of the dust grains,
10
11 i.e., $\lambda = (n\sigma)^{-1}$. The rate is then:
12
13

$$T = n\sigma v \quad (2)$$

14
15
16
17 347 As in ?, by conservation of energy and angular momentum, we assume:
18
19
20

$$\sigma = \pi a^2 [1 \pm 2Ze^2 / (4\pi\epsilon_0 am_i u_i^2)] \quad (3)$$

21
22
23 348 $Ze (> 0$, in this case) represents the charge of the grain and u_i the velocity of
24
25 349 the incident particles. We use the *plus* sign if electrons and *minus* if ions. Even
26
27 350 though most of the bulk mass of the solar wind is due to the ions, from the Ulysses
28
29 351 data, we know that the solar ion density and the total number density of electrons
30
31 352 per cubic centimeter are similar as well as the ion and total electron temperatures.
32
33 353 The solar wind plasma moves as an ensemble of particles and therefore we can
34
35 354 also assume the same speed for both species. Combining Eq.2 and Eq.3 we have
36
37 355 that the maximum number of ion encounters ($\sim 7.43 \text{ day}^{-1}$) is slightly less than
38
39 356 the maximum number of electron encounters ($\sim 7.50 \text{ day}^{-1}$). Ions and electrons
40
41 357 may be captured by the grains, but some of these encounters may also produce loss
42
43 358 of material on the grains by sputtering electrons if the collisions are sufficiently
44
45 359 energetic. Furthermore, if we only assume capture of ions/electrons, the change
46
47 360 rate of ϕ would also be *small* such that a typical grain would require more than
48
49 361 2 months ($\approx 79 \text{ days}$) to change its ϕ by 1 *volt* (7 charges). On the other hand, a
50
51 362 simple capture of ions and electrons seems to turn grains more negative, but since
52
53 363 a fraction of these ions/electrons would produce electron emission, this excess of
54
55 364 negative charge could be compensated by positive charges, and in the long run,
56
57 365 grains could turn slightly more positive considering the contribution of photoion-

1
2
3
4
5
6
7
8
9
366 ization as well. According to ?, dust streams grains' composition is mainly $NaCl$,
10
367 but Sulphur or sulphurous components may be another constituent in the grains.
11
12
368 A minor fraction also shows silicon components which implies that the gossamer
13
14
369 ring cannot be ruled out as a minor source ($\sim 5\%$) of the stream particles. As
15
16
370 reference, we know that for SO_x grains, incident electrons with optimum energies
17
18
371 around 300 eV have yields around 3 (?). Both, the small sizes of dust stream par-
19
20
372 ticles and the low number densities of the solar wind within a few AU of Jupiter,
21
22
373 greatly slow the rate that dust grain acquires electric charges. Accordingly, dust
23
24
374 grain charges may be considered nearly constant during the grains' approximately
25
26
375 week-long journeys to the spacecraft.
27
28

376 4.2. Grain motion

377 Grains that escape from Jupiter, depart from positions near or at the jovian
378 equatorial plane, but since the jovian magnetic field axis is tilted 10° w.r.t. the
379 planet's rotation axis, grains will not necessarily follow escape trajectories along
380 or close to the jovian equatorial plane. However, though the magnetic axis may
381 keep a constant tilt w.r.t. the rotation axis and the ecliptic plane, its relative incli-
382 nation w.r.t. the Sun varies as Jupiter moves about it. This implies that, at least,
383 for the jovian grains that Ulysses detected inside Jupiter's orbit and that escape
384 towards the Sun or near the Sunward direction, the inclination of their escape tra-
385 jectories w.r.t. the ecliptic plane may depend on the position of the planet along its
386 orbit. For these grains, the inclinations of their escape trajectories from the mag-
387 netosphere are likely within a $\sim 20^\circ$ interval centered at the ecliptic. Data shows
388 (Fig. 3b) that the number of detected dust streams increased when the spacecraft
389 was, not only near the planet, but close to the ecliptic plane. Nevertheless, dust
390 streams were also detected at medium and high jovigraphic latitudes and these

1
2
3
4
5
6
7
8
9
391 large detection angles suggest that the dust grains' motion is largely deflected
10
392 from their original ejection direction while they travel through the interplanetary
11
12
13
393 space.

14
394 A simple and satisfactory first explanation of the dust stream production, which
15
16
395 we complement with actual data in this section, was published by ?. These au-
17
18
396 thors assumed that the motion of the charged dust grains ejected from the mag-
19
20
397 netosphere of Jupiter is only perturbed along the direction perpendicular to the
21
22
398 ecliptic plane. This theoretical model states that an alternate periodic perturbation
23
24
399 due to the IMF variation connected with the solar rotation leads to a periodic up-
25
26
400 ward and downward oscillation in the dust particles' trajectories perpendicular to
27
28
401 the ecliptic plane. The largest deflections occur when grains undergo the influence
29
30
402 of the enhanced IMF of CIRs and CMEs and thus, stronger CRs lead to stronger
31
32
403 deflections.

33
34
404 The influence of the IMF on the charged dust grains not only depends on the
35
36
405 IMF strength (see Fig. 6) but also on the solar wind speed. Furthermore, it also
37
38
406 strongly depends on the direction of motion of the grains with respect to this field.
39
40
407 This direction is defined by the departing position of the grains around Jupiter
41
42
408 when they escape from the jovian magnetosphere, expressed by the jovigraphic
43
44
409 longitude L .

45
46
410 The grains move along increasing spiral trajectories around Jupiter inside the
47
48
411 jovian magnetosphere (?). Due to conservation of angular momentum, the tan-
49
50
412 gential component of their velocity declines as the radial component grows while
51
52
413 the grains move away from Jupiter. It drops to quite small values at the limits of
53
54
414 the magnetosphere. Thus we can assume that the grain departing longitude is held
55
56
415 fairly constant outside the magnetosphere.

1
2
3
4
5
6
7
8
9
10 Ahead we describe the interaction of a test dust grain with the IMF in terms
11 of jovian geometric parameters as well as solar wind parameters in the vicinity of
12 Jupiter. We start with the electromagnetic force as driving force (in MKS):
13
14

$$\mathbf{F} = Q\mathbf{v}' \times \mathbf{B} \quad (4)$$

15
16
17
18
19 where \mathbf{B} is the IMF vector essentially represented by its tangential component
20 $B_{t_{IMF}}$ and \mathbf{v}' is the relative velocity of the dust grains with respect to the IMF. c
21 ($= 2.99 \times 10^8 \text{ m s}^{-1}$) is the speed of light. The relative velocity of the grains depends
22
23 on their velocity v with respect to Jupiter and the velocity of the solar wind V as
24
25 well as on the longitude L . Again, the radial velocity of grains can be assumed
26
27 constant since only weak forces act on the grains along the radial direction and
28
29 the magnitude of \mathbf{v}' can be defined as follows:
30
31
32
33
34

$$v' = V + v \cos L \quad (5)$$

35
36
37 According to the assumptions made, the magnitude of Equation 4 is:
38
39

$$F = Qv' B_{t_{IMF}} \quad (6)$$

40
41
42
43 Note that this force is calculated from the data and it is displayed in the sixth
44 panel of Fig. 1a to Fig. 1m (in arbitrary units), thus giving a better idea of the
45
46 deflection direction. Grains feel a stronger force under the influence of a com-
47
48 pression region and a less intense force under average IMF conditions. The polar-
49
50 arity of the solar magnetic field defines whether particles are deviated upwards or
51
52 downwards with respect to the ecliptic plane. From Eq. 6 the upward/downward
53
54 acceleration is given by:
55
56
57
58
59
60
61
62
63
64
65

$$\alpha = \left(\frac{\phi}{\pi \rho k a^2} \right) v' B_{t_{IMF}} = 0.132 v' B_{t_{IMF}}, \quad (7)$$

where $k = 8.987 \times 10^9 N m^2 C^2$. We have assumed the same typical spherical dust particle values as in equations (2) and (3). For the sake of simplicity, in the second member of this former equation, the units of the magnetic field were adjusted to nanoteslas and the speed's units to hundreds of kilometers. Since, under our general assumption, the force is perpendicular to the direction of motion, we can assume, following Hamilton and Burns (1993), that dust particles, whose average motion is along the ecliptic plane, recede from the ecliptic plane in sections of parabolic trajectories. Unlike Hamilton and Burns (1993), who assumed significantly larger grains with far slower speeds, here one segment of a parabola usually suffices. Accordingly, the vertical position z of a grain can be described by:

$$z = \pm \frac{1}{2} \alpha t^2 = \pm 0.066 v' B_{t_{IMF}} t^2. \quad (8)$$

Since the distance travelled by dust in the ecliptic plane is simply vt , we can easily obtain the jovigraphic latitude as a function of time:

$$\beta = \pm \tan^{-1} \left[0.066 B_{t_{IMF}} \left(\frac{V + v \cos L}{v} \right) t \right]. \quad (9)$$

Eq. 9 summarizes the relationships between the physical properties that play important roles in the production and dynamics of dust streams. It also makes some interesting predictions that we might see in the data. The most important point is that β is a function of L , the angle between the Sun and the dust trajectory projected into the ecliptic; if $V \approx v$, it is a strong function of L . Thus, all else being equal, dust streams can be expected to be deflected more strongly out of

1
2
3
4
5
6
7
8
9
10 453 the ecliptic plane when they are directed toward the Sun ($L = 0$). Under average
11 454 IMF conditions, i.e. $B_{IMF} \approx 0.5$ nT -with a single polarity-, dust grains can gain a
12
13 455 latitude $\beta \approx \pm 7^\circ$ in only 2 days; this is increased to $\beta \approx \pm 25^\circ$ if, while escaping,
14
15 456 the grains encounter an average CIR with its enhanced B_{IMF} .

16
17 457 The dust particles that escape along the Jupiter-Sun line ($L = 0^\circ$) are the fastest
18
19 458 in the frame of reference of the moving IMF and therefore the effects of this field
20
21 459 will be the greatest with respect to other grains ejected in different directions. It is
22
23 460 tempting to argue, therefore, that CIRs have a greater effect for dust streams pro-
24
25 461 jected toward the Sun, however this is not so. The time that a dust stream remains
26
27 462 in a CIR of given radial length r_{CIR} is simply $t = r_{CIR}/(V + v \cos L)$ which, when
28
29 463 inserted into Eq. 9, cancels out the longitude dependence. Sunwardly-projected
30
31 464 dust streams experience stronger deflection forces, but for a shorter amount of
32
33 465 time. In this case, the detector geometry, which is not considered here, probably
34
35 466 plays a major role (?).

36
37 467 In any case, these effects will be greater inside the compression regions than
38
39 468 under average IMF conditions. In particular, for the dust grains ejected from the
40
41 469 day side of the magnetosphere, the relative perpendicular velocity will be maxi-
42
43 470 mum when $L = 0^\circ$ ($v' = 2v_{sw}$) and minimum when $L = 90^\circ$.

44
45
46 471
47 472 The grains ejected from the night side of the magnetosphere are another in-
48
49 473 teresting case, since their perpendicular velocity with respect to the IMF is, on
50
51 474 average, much smaller than on the day side. In particular, near $L \sim 180^\circ$ the
52
53 475 perpendicular velocity is very small and at $L = 180^\circ$ it nearly vanishes because
54
55 476 $v \approx V$. Thus, grains are only slightly affected by the IMF, receding from Jupiter
56
57 477 along nearly straight-line trajectories.

1
2
3
4
5
6
7
8
9
10
11
12
13
14
15
16
17
18
19
20
21
22
23
24
25
26
27
28
29
30
31
32
33
34
35
36
37
38
39
40
41
42
43
44
45
46
47
48
49
50
51
52
53
54
55
56
57
58
59
60
61
62
63
64
65

478 5. CONCLUSIONS

479 In this work we have done a direct comparison of the Ulysses solar wind,
480 IMF and dust data in order to have a better picture of how the motion of the dust
481 grains ejected by Jupiter is modulated to produce the jovian dust streams. This
482 demonstrates how relevant the periodic intensity variations of the solar wind and
483 the IMF are in this modulation. We highlight some important and evident features
484 from the data:

485 *First*, there is always a previous high IMF event associated with an observed
486 dust stream. These events are, in most cases, corotating interaction regions, and
487 in a few cases, coronal mass ejections (Fig. 1).

488 *Second*, the duration of each dust stream roughly matches the duration of a
489 precedent CR (Fig. 5).

490 *Third*, the occurrence of each dust stream and the occurrence of the previous
491 CR are separated by a time interval that depends on the distance to the planet (Fig.
492 6).

493 *Fourth*, the intensity of the compression regions (CRs) is connected to the
494 intensities of the successive dust streams such that intense events produce intense
495 streams and weak events produce weak dust streams or no dust streams at all (Fig.
496 7). This hold at least in the case of the first flyby data. There is no such correlation
497 in the second flyby, indicating the importance of detector geometry.

498 Out of these facts, we can conclude that strong enough CRs are key in the de-
499 tection of the so called jovian dust streams, which are an enhancement in the local
500 dust density observed by the spacecraft. Evidence seems to indicate that CIRs and
501 CMEs, through strong vertical deflections, modify this local dust density. Further-
502 more, enhancements in the dust flux seem to occur when the heliospheric current

1
2
3
4
5
6
7
8
9
10
11
12
13
14
15
16
17
18
19
20
21
22
23
24
25
26
27
28
29
30
31
32
33
34
35
36
37
38
39
40
41
42
43
44
45
46
47
48
49
50
51
52
53
54
55
56
57
58
59
60
61
62
63
64
65

503 sheet sweeps across the spacecraft. Depending on the polarity of the interplanetary magnetic field, which varies with the solar cycle, dust may be attracted to
504 or repelled from the current sheet. The complicated interplay between CRs, and
505 the current sheet - as well as the dust detector's pointing geometry - likely can account for the fact that some strong CRs are not followed by streams. Furthermore,
506 some small dust streams may not have been noticed in the dust data; here we have
507 confined our analysis to the dust streams identified by ? and ? that account for
508 those streams that have the highest probability of occurrence. However, notice
509 that other possible weak and short dust streams can be seen in the data (e.g. Fig.
510 1a: Day 329, Fig. 1b: Day 57-60, Fig. 1d: Day 264-267 and Fig. 1h: Day 57,
511 101).

514 The distance from the source and geometry seems to play a quite important
515 role as can be seen in the correlations shown in Figs. 5-7. On the one hand,
516 the first flyby data, where the detection was closer to Jupiter, show acceptable
517 coefficients, while in the case of the second flyby, the correlations decrease. A
518 possible explanation is that the longer the grains travel away from Jupiter, the
519 more coupled with the IMF the grains will be. If true, it is probable that in the
520 long run a good portion of the grains that compose the dust streams would be
521 eventually dragged by the IMF.

522 Of course, there are other variables that affect jovian dust stream properties,
523 such as the volcanic activity of Io, the plasma density in the torus or the general plasma conditions around Jupiter. For example, surface changes on Io give
524 evidence of not only a continuous, but also a variable volcanic activity (?) that
525 modulates the amount of material - dust included - that is transported away from
526 the satellite. On the other hand, asymmetries in the temperature profile in the
527

1
2
3
4
5
6
7
8
9 528 plasma torus may also vary the charging conditions, affecting the dust flux which
10 is ejected to the interplanetary medium (?).
11

12
13 530 Finally, we conclude that the dynamical effects on the jovian dust streams we
14 have investigated here mainly apply within a few astronomical units from Jupiter
15 531 such that dust grains flight times are short. A description of the long term effects of
16 the solar wind will be subject of a future work. Our investigation of the jovian dust
17 532 streams will be applicable to the saturnian dust streams as well, since the same
18 physical mechanisms are at work at Saturn. Furthermore, dust streams should also
19 533 form at the other giant planets Uranus and Neptune, provided that a sufficiently
20 strong dust source exists. This study may also stimulate new investigations of
21 534 the dust-magnetosphere interaction within the jovian magnetosphere as measured
22 with Galileo. We also hope that the data shown in Figure 1 will be useful for
23 535 further studies of the dust stream formation mechanisms.
24
25
26
27
28
29
30
31
32
33
34
35
36

37 541 Acknowledgements:

38
39 542 Part of this work was carried out at the Jet Propulsion Laboratory under con-
40 tract with NASA. Part of this work was also carried out at the Max-Planck-Institut
41 543 für Sonnensystemforschung in Katlenburg-Lindau during a research stay. The
42 authors thank Reiner Schwenn for his support in the CIRs and CMEs identifica-
43 544 tion. A. Flandes thanks D. Maravilla and her support through the project DGAPA
44 IN111207.
45
46
47
48
49
50
51
52
53
54
55
56
57
58
59
60
61
62
63
64
65

1
2
3
4
5
6
7
8
9
10
11
12
13
14
15
16
17
18
19
20
21
22
23
24
25
26
27
28
29
30
31
32
33
34
35
36
37
38
39
40
41
42
43
44
45
46
47
48
49
50
51
52
53
54
55
56
57
58
59
60
61
62
63
64
65

548 **6. REFERENCES**

Accepted manuscript

549 7. FIGURE CAPTIONS

550 Figure 1a to Fig. 1m. Ulysses Solar wind, interplanetary magnetic field and
 551 dust data from both Jupiter flybys: Solar wind speed V , proton density N_p , Proton
 552 maximum temperature T_p , IMF intensity $|B|$ and azimuthal angle Φ . Next is the
 553 vertical Lorentz force F_n in arbitrary units and finally the dust impact rate. Data
 554 are organized in multiple integers of solar rotation periods (~ 27 days) to highlight
 555 periodicities. The dark gray numbered bars in the bottom panel indicate the dust
 556 stream peaks in every case. The gray stripes indicate compression regions. The
 557 darker stripes indicate those events that precede and are associated to dust streams.
 558 Fig 1b shows a gap in the data series between days 33 and 46. Jovicentric distance
 559 is shown at the top.

560 Figure 2. Projection of the orbit of the Ulysses spacecraft on the XZ plane (Top
 561 panel) and the XY plane (ecliptic plane, bottom) during the second Jupiter flyby.
 562 The positions of Ulysses and Jupiter at their closest approach (5 February 2004,
 563 distance $r = 0.8\text{AU}$) are indicated. Jupiter defines the origin of this coordinate
 564 system. β and L represent the jovigraphic latitude and longitude angles with the
 565 Jupiter-Sun direction as their starting measuring position or zero. At the shown
 566 positions $\beta = +54.1^\circ$ and $L = +73.4^\circ$.

567 Figure 3. Ulysses angular position with respect to Jupiter during the first (top)
 568 and second (bottom) Jupiter flybys (stream 201 is not included). The dust impact
 569 rate is displayed to highlight the dust flux variation with distance to Jupiter. The
 570 jovigraphic latitude, β , is measured with respect to the jovian equatorial plane.
 571 Positive latitudes correspond to the northern hemisphere and negative latitudes
 572 to the southern hemisphere. Jovigraphic longitudes are measured with respect to

1
2
3
4
5
6
7
8
9
10 573 the Jupiter-Sun line ($L = 0^\circ$). Positive longitudes are measured in the counter-
11 574 clockwise directions and vice versa (Fig.2).

12
13
14 575 Figure 4. Comparison of the joventric distance (top), the dust stream flux
15 576 (middle) and CR-dust stream offset for both flybys. plus symbols and continuous
16 577 lines represent the first flyby and triangles and dotted lines represent the second
17 578 flyby.

18
19
20
21
22
23 579 Figure 5. Least squares trend of the durations of the high IMF events (Δt_C)
24 580 and the dust streams (Δt_s) during both Ulysses Jupiter flybys. The duration of
25 581 each dust stream seems to be a consequence of the duration of CRs. We use the
26 582 stream numbers as markers for a better analysis. The smaller number size of the
27 583 markers indicates $\beta < 0$. Typical error bars are shown at the bottom right of the
28 584 figure. R stands for the correlation coefficient of the fit in each case. We highlight
29 585 that due to their atypically long durations, streams 212, 213 and 214 were not
30 586 considered in the correlation, but they are shown for comparison.

31
32
33
34
35
36
37
38
39 587 Figure 6. Least squares trend of the dust stream detection distance r from
40 588 Jupiter vs. the time delay Δt between the beginning of the precedent high IMF
41 589 events and the beginning of the most probable dust stream from the 1991-1992
42 590 and 2002-2005 Ulysses data set. Smaller symbols indicate $\beta < 0$. Typical error
43 591 bars are shown at the bottom right of the figure. The correlation coefficient R is
44 592 given in each case.

45
46
47
48
49
50
51 593 Figure 7. Dust stream flux versus maximum magnetic field intensity of the
52 594 precedent event. The dust flux has been multiplied by the square of the distance
53 595 to Jupiter to correct for the varying spacecraft distance from Jupiter. The top plot

1
2
3
4
5
6
7
8
9
10
11
12
13
14
15
16
17
18
19
20
21
22
23
24
25
26
27
28
29
30
31
32
33
34
35
36
37
38
39
40
41
42
43
44
45
46
47
48
49
50
51
52
53
54
55
56
57
58
59
60
61
62
63
64
65

596 (first flyby) shows a least squares fit trend that indicates a correlation, nevertheless,
597 the second flyby (bottom plot) shows no correlation.

Accepted manuscript

Table 1: Dust streams parameters and related high IMF events identified in the Ulysses data set: Flyby/N: Stream identification number (1); dust stream peak year and day (2); Δt_s : dust stream duration (3); r: jovicentric distance (4); β : jovigraphic latitude (5); L: jovigraphic longitude (6); $F r^2$: dust stream flux (7); EVENT: precedent CIR (normal text) or CME (italics) occurrence and duration (8); Δt_C : Event duration (9); Δt : period between precedent event-peak and following dust stream peak (10); $|B|$: Event maximum magnetic field intensity (11). Data in columns (1) to (5) and (7) were taken from ? and ?.

Flyby/N	Year/day	Δt_s [days]	r [AU]	β [°]	L [°]	$F r^2$ [$m^{-2}s^{-1}AU^2$]	EVENT [year/days]	Δt_C [days]	Δt [days]	$ B_{max} $ [nT]
(1)	(2)	(3)	(4)	(5)	(6)	(7)	(8)	(9)	(10)	(11)
101	91/267.8	3.2	1.1	1.6	10.55	0.0109	91/263.7 - 266.7	3.1	2.5	4.55
102	91/346.8	0.4	0.5	1.9	17.28	0.0094	91/345.0 - 349.7	4.8	1.6	4.91
103	91/358.2	0.8	0.4	2.2	18.38	0.0017	91/356.1 - 359.4	3.4	1.8	2.45
104	92/007.2	0.4	0.3	2.3	19.79	0.0024	92/006.0 - 009.6	3.6	1.0	4.06
105	92/019.3	2.4	0.2	2.7	21.32	0.0010	92/018.0 - 021.3	3.2	0.1	1.70
106	92/070.9	1.4	0.3	-35.9	87.55	0.0031	92/065.7 - 069.1	3.4	4.5	1.65
107	92/098.7	2.5	0.5	-35.9	85.22	0.0010	92/090.8 - 095.4	4.7	6.7	2.08
108	92/126.2	2.3	0.7	-35.9	83.32	0.0025	92/119.0 - 122.1	3.1	6.1	0.99
109	92/155.3	4.5	0.9	-35.1	81.32	0.0028	92/144.1 - 150.7***	6.5	8.9	2.96
110	92/247.0	9.0	1.6	-35.8	75.66	0.0015	92/226.2 - 234.1*	7.9	16.3	3.00
111	92/292.2	4.3	2.0	-35.7	72.54	0.0058	92/279.7 - 285.4	5.8	10.4	3.52
201	02/332.5	2.9	3.4	44.0	-36.39	0.0341	02/324.4 - 325.8	1.4	6.7	1.15
202	03/192.0	6.6	1.8	58.0	-48.28	0.0383	03/176.0 - 184.4***	8.4	12.7	3.76
203	03/238.1	5.5	1.5	64.0	-46.20	0.0073	03/226.9 - 235.0***	8.1	8.5	3.95
204	03/263.6	1.8	1.4	67.0	-42.01	0.0024	03/257.9 - 261.9	4.0	4.8	2.38
205	03/288.3	7.5	1.2	72.0	-33.58	0.0056	03/276.0 - 286.3	10.3	8.5	2.67
206	03/315.7	1.2	1.1	76.0	-10.30	0.0169	03/310.7 - 314.1	3.4	4.4	4.22
207	03/337.5	2.7	0.9	76.0	22.82	0.0258	03/333.5 - 336.0	2.5	2.6	3.80
208	03/364.5	3.0	0.9	70.0	56.91	0.0011	03/360.5 - 364.2	3.7	2.5	4.49
209	04/025.6	4.1	0.8	57.0	71.68	0.0042	04/019.9 - 024.6	4.7	3.7	5.24
210	04/050.0	3.7	0.8	44.0	77.82	0.0017	04/045.6 - 049.9	4.3	2.6	2.88
211	04/080.2	8.1	0.9	29.0	81.20	0.0009	04/074.3 - 082.1	7.8	1.8	2.58
212	04/155.3	10.0	1.2	3.0	82.07	0.0443	04/150.6 - 155.0	4.4	0.3	2.46
213	04/169.7	12.0	1.3	0.0	81.68	0.1385	04/161.3 - 166.1	4.8	2.4	1.44
214	04/181.0	10.0	1.4	-2.0	81.32	0.0640	04/174.5 - 179.1	4.6	1.5	2.08
215	04/190.2	2.4	1.5	-4.0	80.99	0.0028	04/187.8 - 192.2	4.4	1.2	1.92
216	04/202.0	3.0	1.5	-5.0	80.53	0.0038	04/199.0 - 201.9	2.9	1.5	2.87
217	04/215.8	6.9	1.6	-7.0	79.94	0.0039	04/203.4 - 207.2**	3.8	8.9	0.78
218	04/231.0	6.0	1.8	-9.0	79.13	0.0013	04/225.9 - 229.1	3.2	2.1	2.21
219	04/246.0	4.0	1.8	-11.0	78.46	0.0024	04/234.5 - 241.0	6.5	9.5	3.04
220	04/302.5	5.0	2.2	-16.0	75.35	0.0058	04/286.5 - 290.8	4.3	13.5	1.48
221	04/331.8	1.0	2.4	-18.0	73.62	0.0068	04/323.8 - 325.6	1.8	7.5	0.81
222	04/362.3	1.2	2.6	-19.0	71.71	0.0051	04/354.2 - 355.5	1.3	7.5	2.64
223	05/044.2	5.0	3.0	-21.0	68.53	0.0089	05/027.8 - 033.0	5.2	13.9	5.34
224	05/082.6	3.9	3.2	-23.0	66.97	0.0045	05/071.7 - 075.9	4.2	9.0	3.08
225	05/123.9	2.0	3.5	-24.0	63.11	0.0088	05/120.8 - 125.4	4.6	2.1	2.97
226	05/175.3	3.0	3.8	-25.0	59.44	0.0222	05/169.6 - 172.2**	2.6	4.2	2.88
227	05/209.8	3.0	4.0	-26.0	56.93	0.0475	05/192.7 - 194.4	1.7	15.6	2.60
228	05/228.6	4.0	4.1	-26.0	55.44	0.1462	05/214.2 - 217.4	3.2	12.4	6.95

* Very close and successive CIRs separated by few days that are considered as a single event.

** It is not clear whether it is a CIR or a Coronal Mass Ejection (CME) or both.

*** CIR preceded by a CME considered as a single event.

Fig.1a First Flyby, Year 1991, Days 257–365

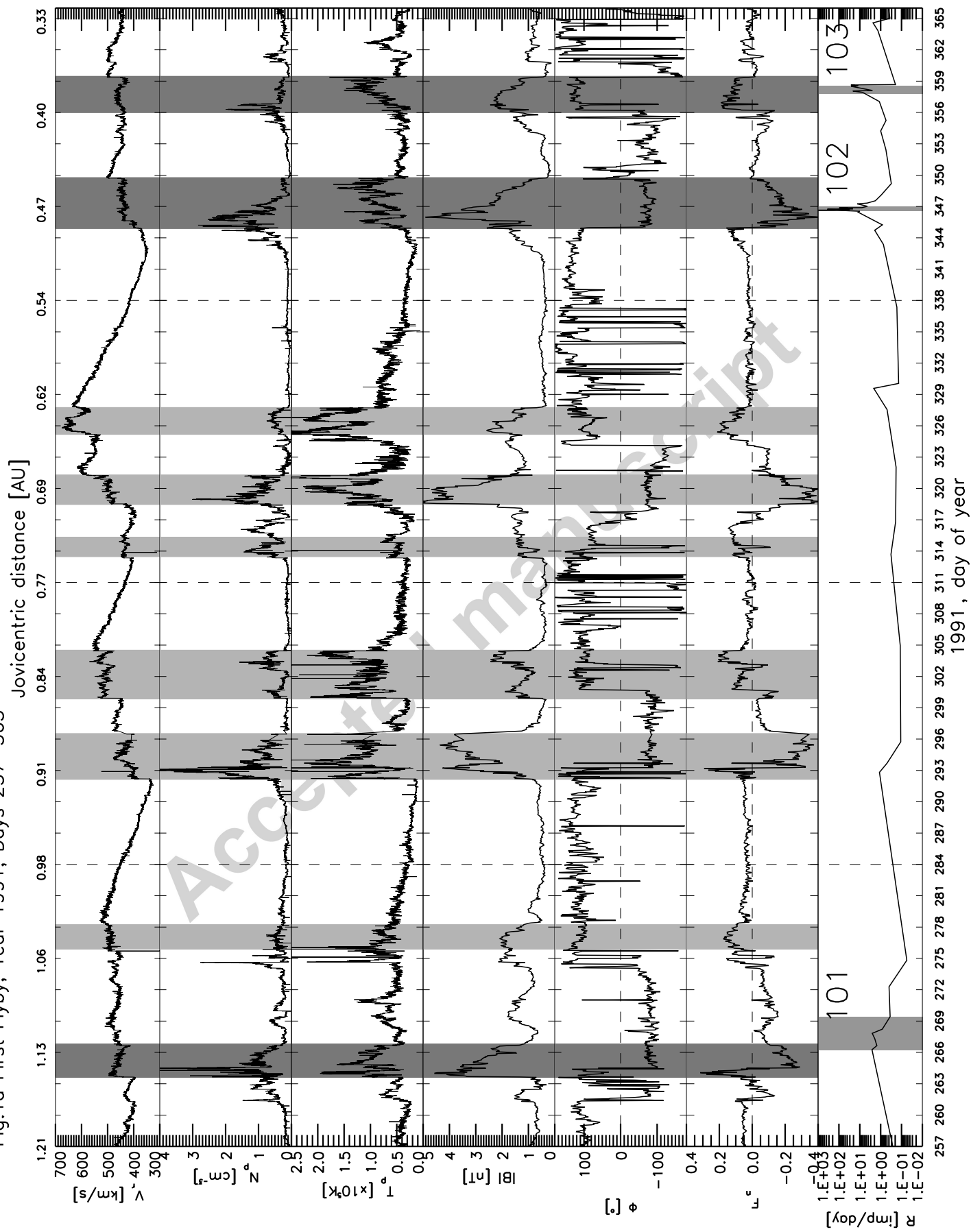


Fig.1b First Flyby, Year 1992, Days 0–108

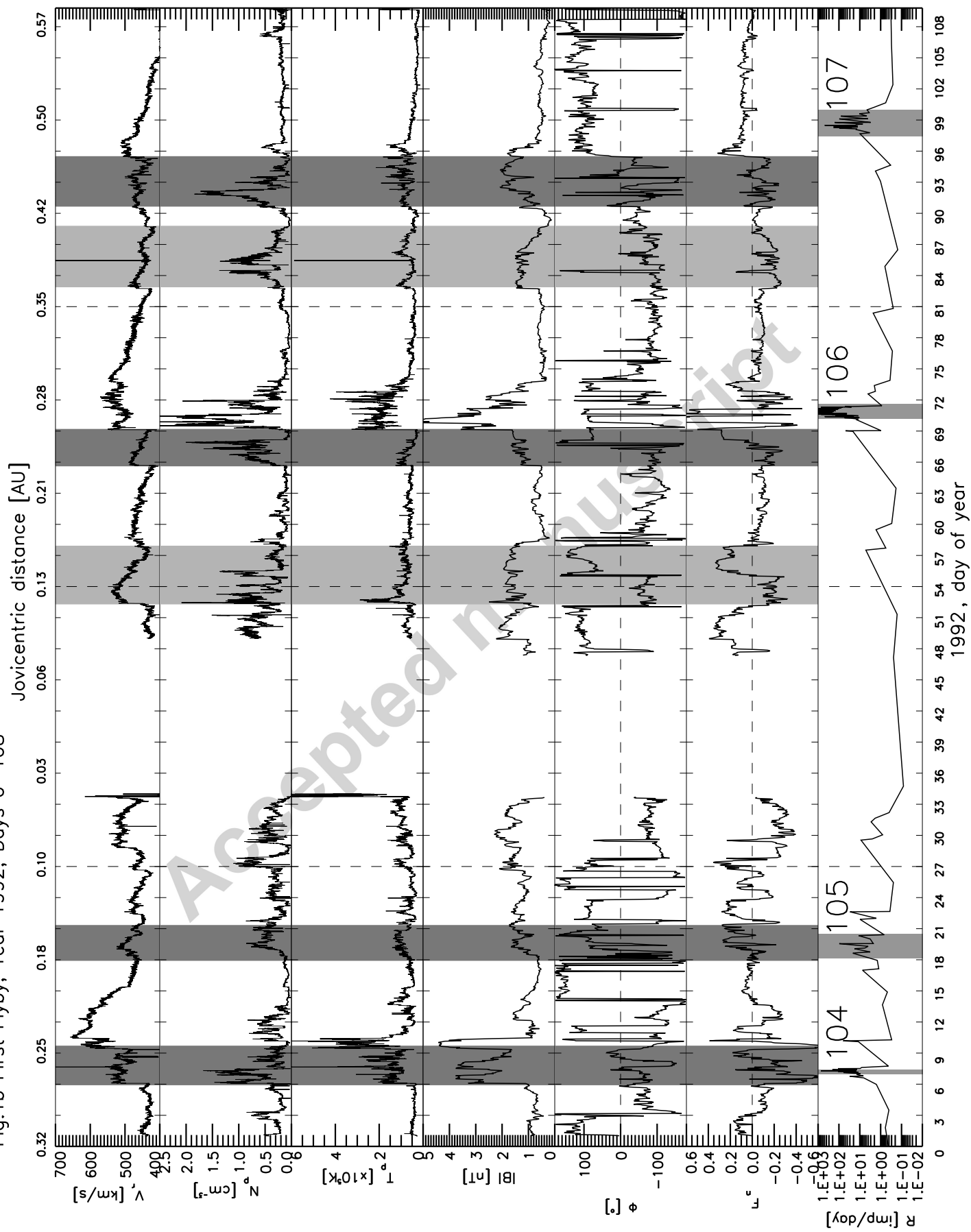


Fig.1c First Flyby, Year 1992, Days 108–216

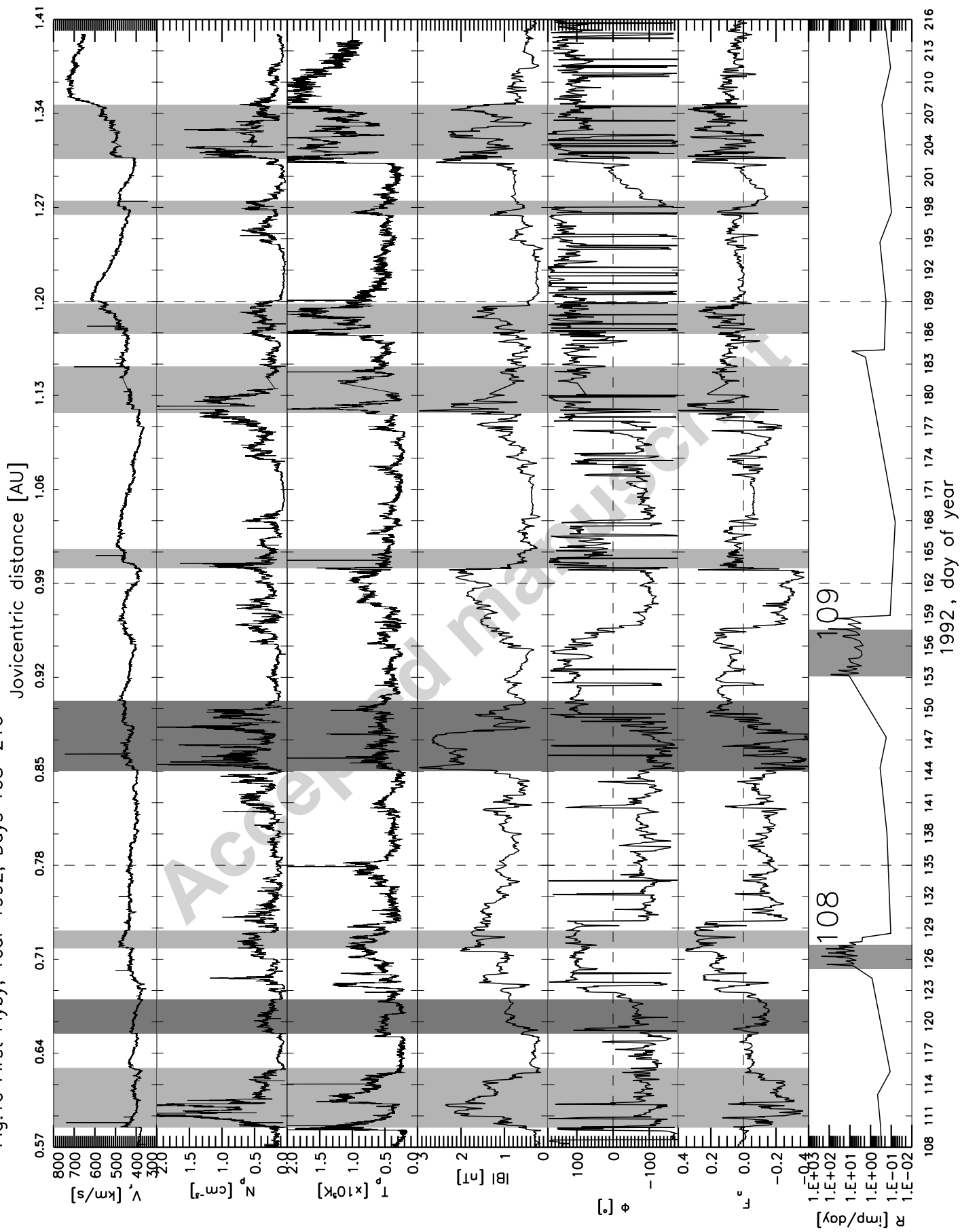


Fig.1d First Flyby, Year 1992, Days 216–324

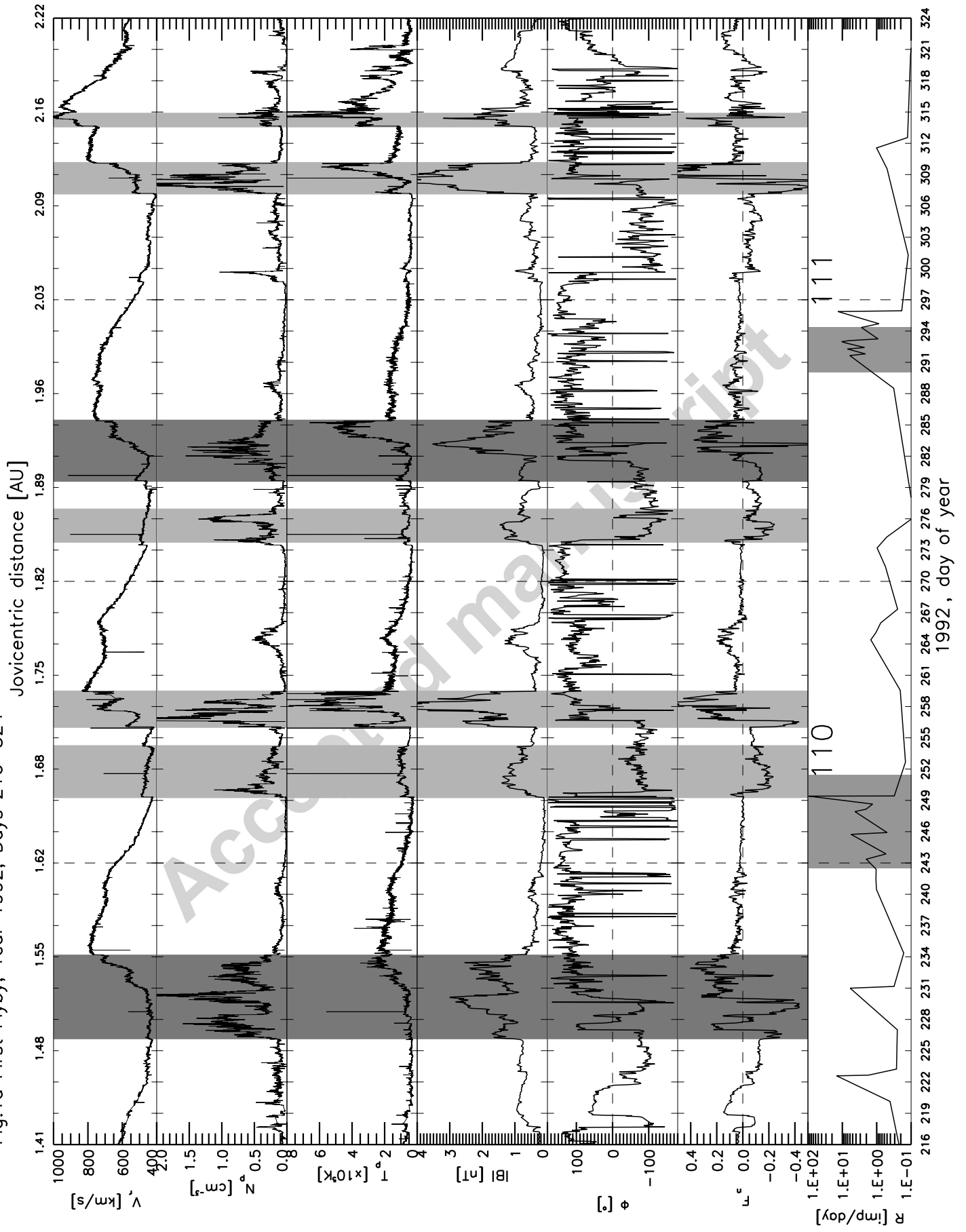


Fig.1e Second Flyby, Year 2002, Days 284–338

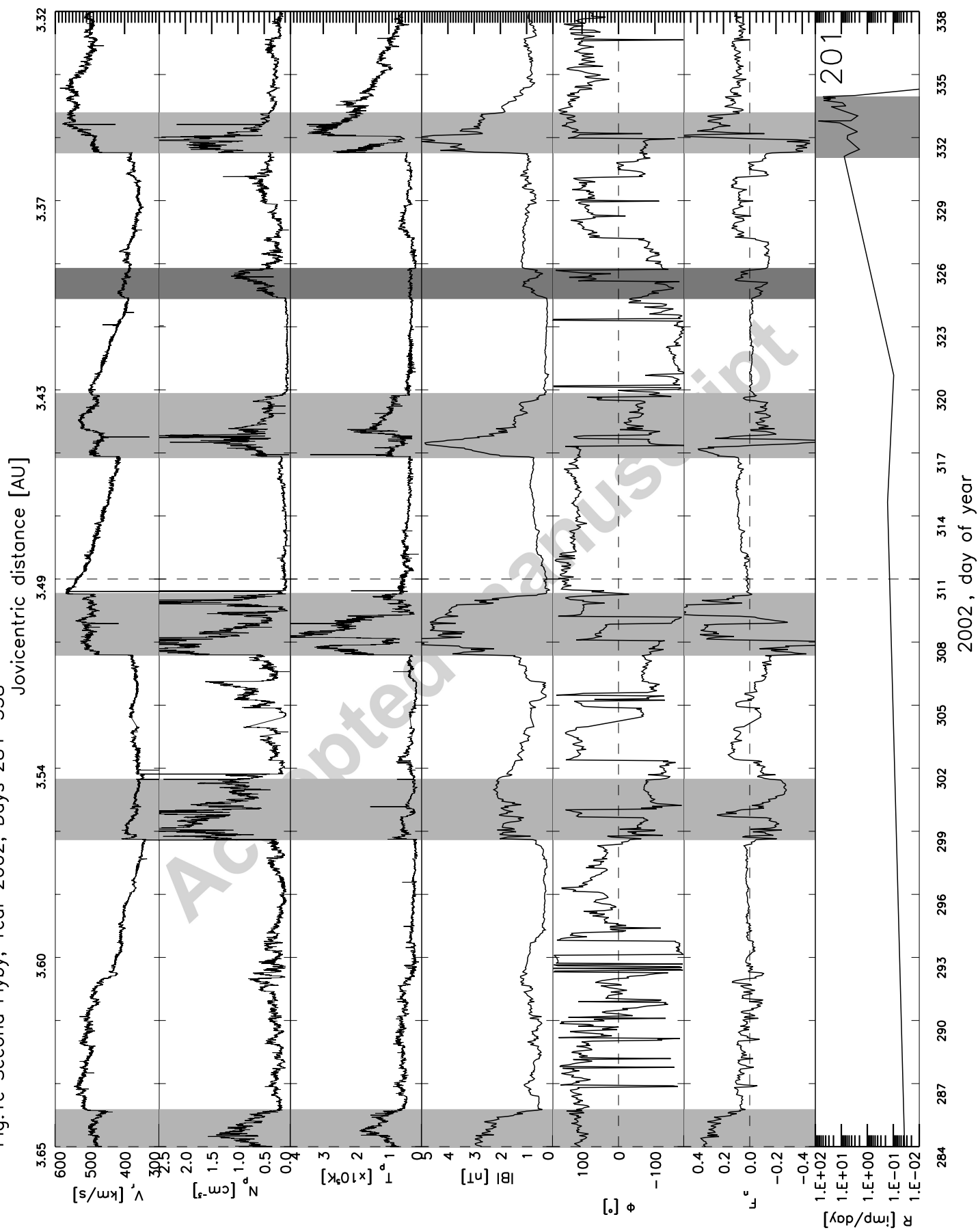


Fig.1f Second Flyby, Year 2003, Days 149–257

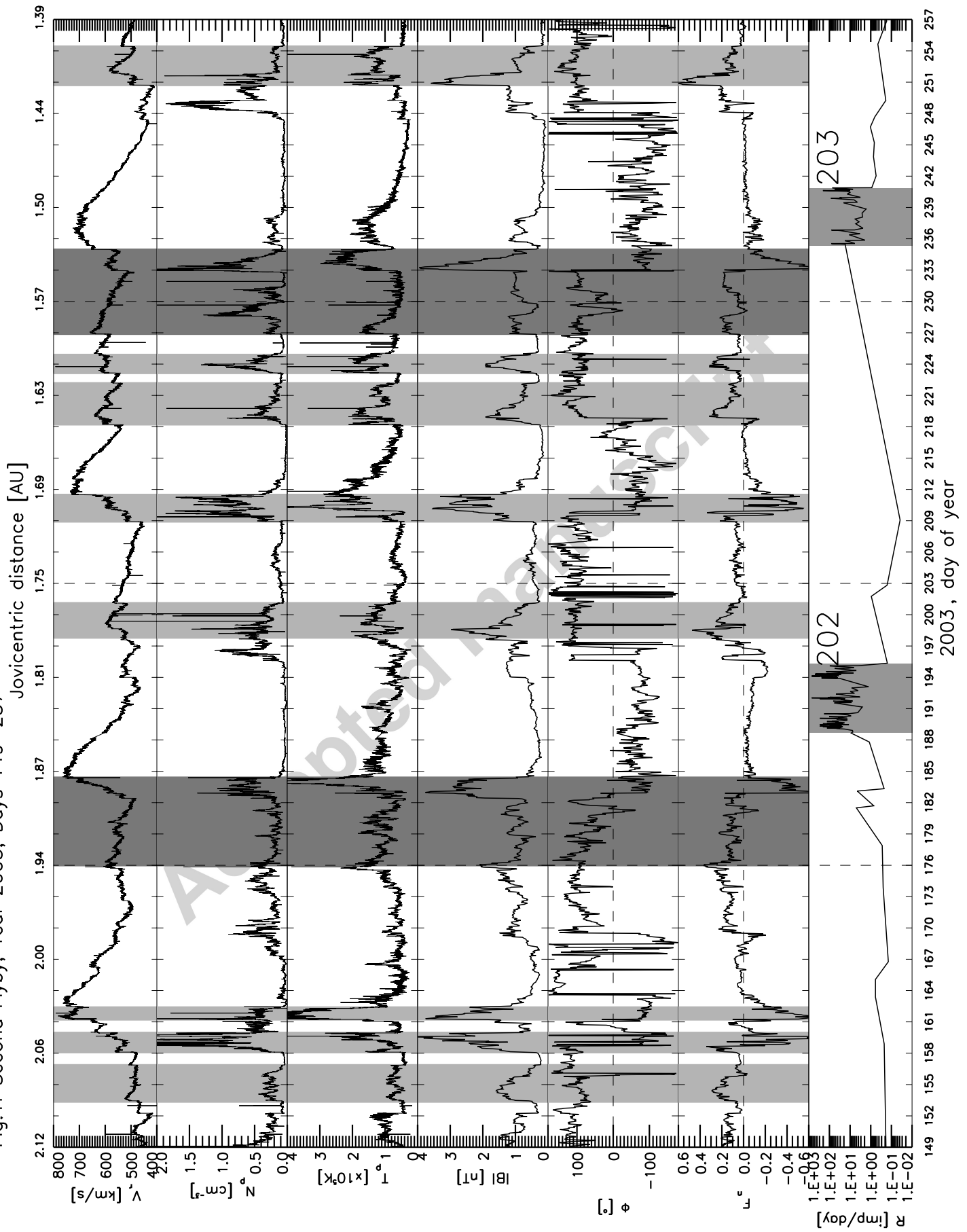


Fig.1g Second Flyby, Year 2003, Days 257–365

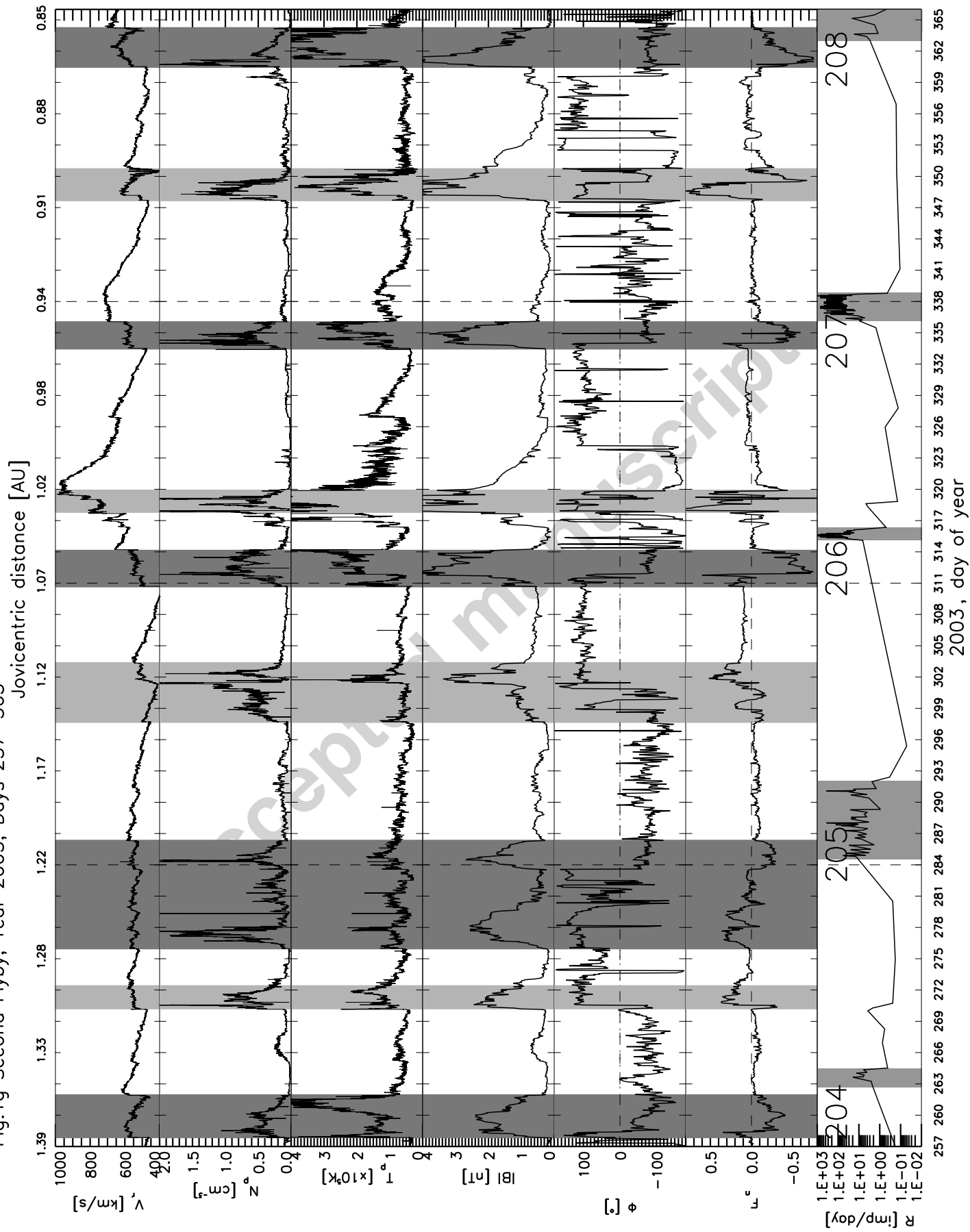


Fig.1h Second Flyby, Year 2004, Days 0–108

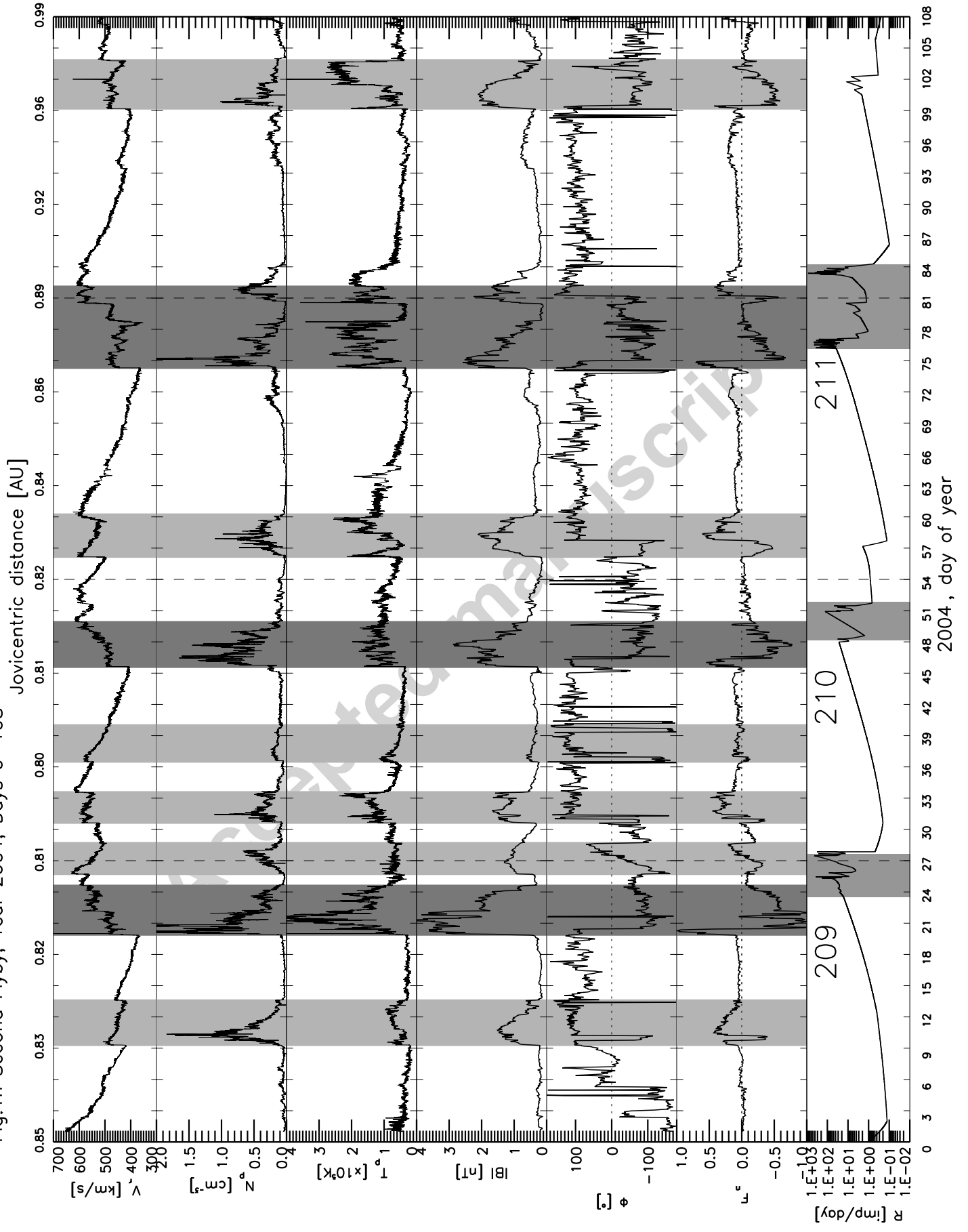
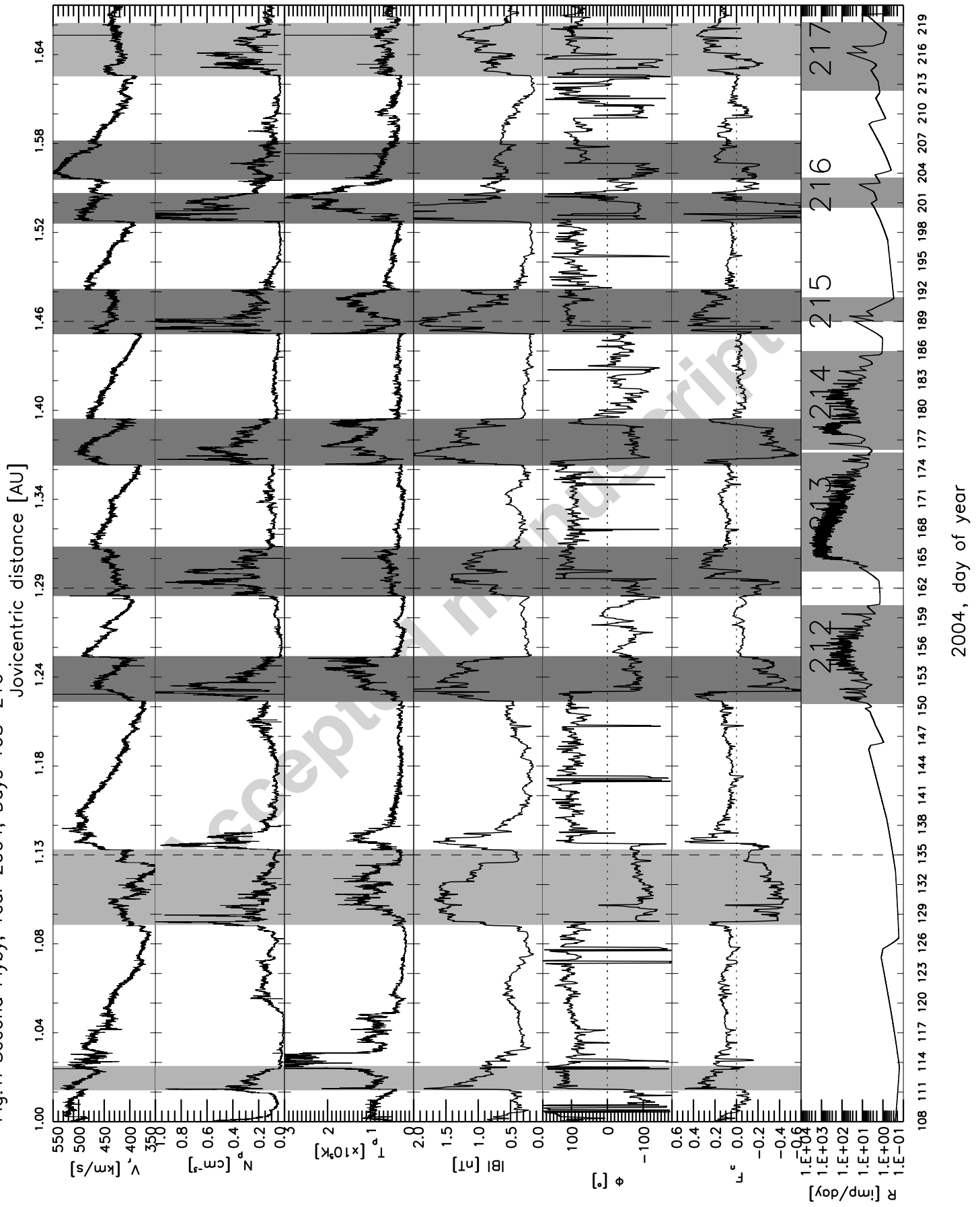
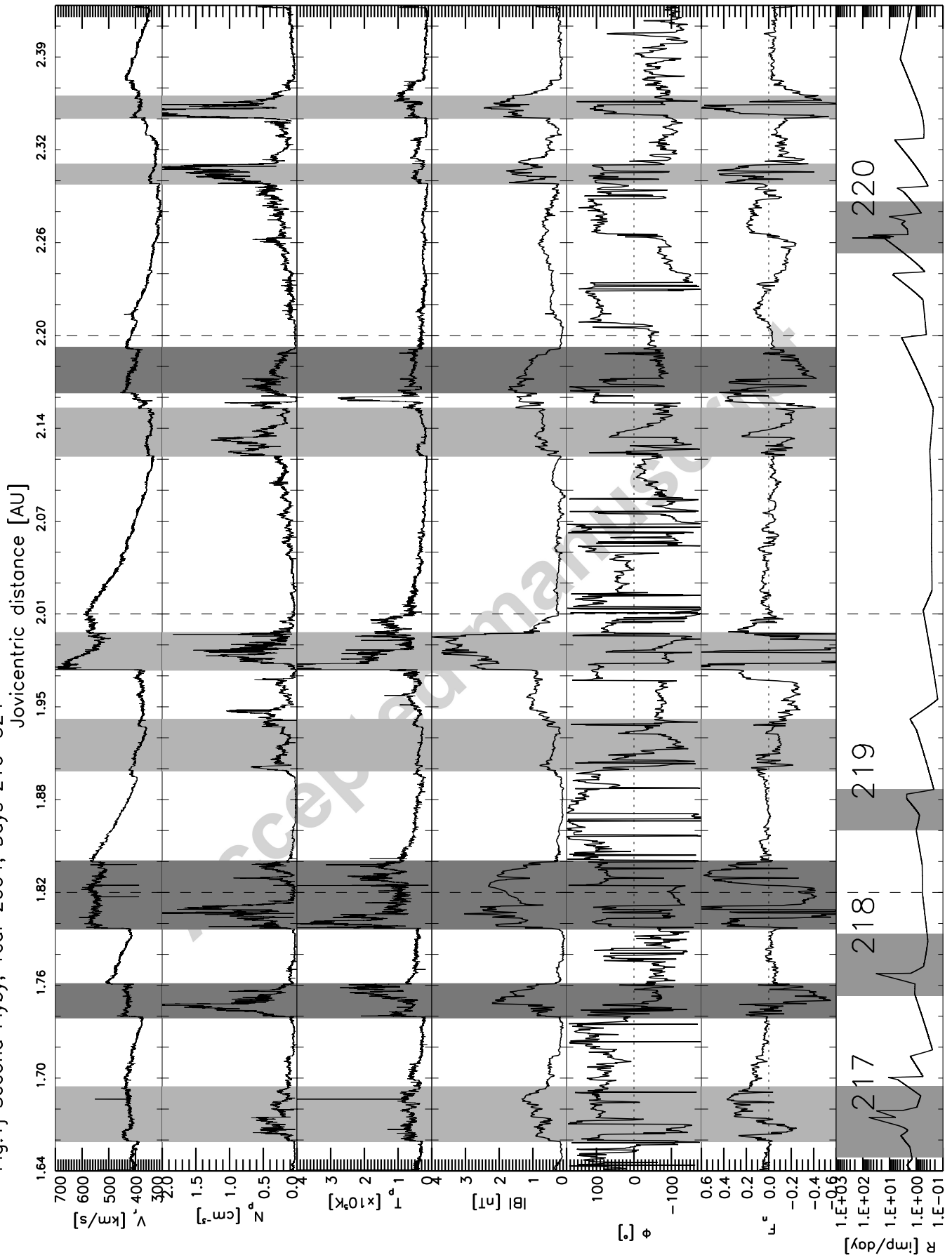


Fig. 1i Second Flyby, Year 2004, Days 108–216



2004, day of year

Fig.1j Second Flyby, Year 2004, Days 216–324



211 214 217 220 223 226 229 232 235 238 241 244 247 250 253 256 262 265 268 271 274 277 280 283 286 289 292 295 298 301 304 307 310 313 316 319 322

2004, day of year

Fig.1k Second Flyby, Year/Days 2004:324–365 – 2005:0–66

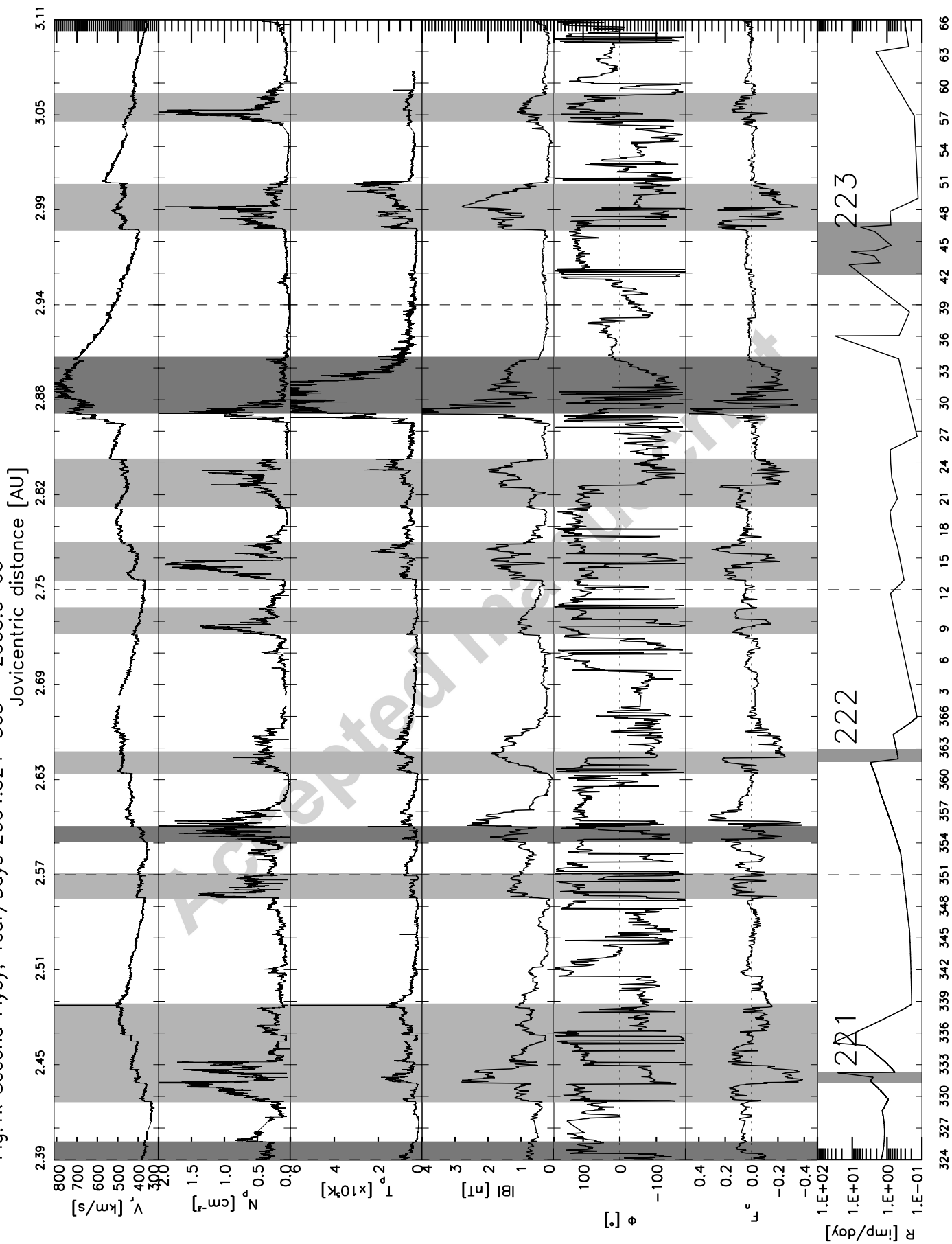


Fig. 11 Second Flyby, Year 2005, Days 66–174

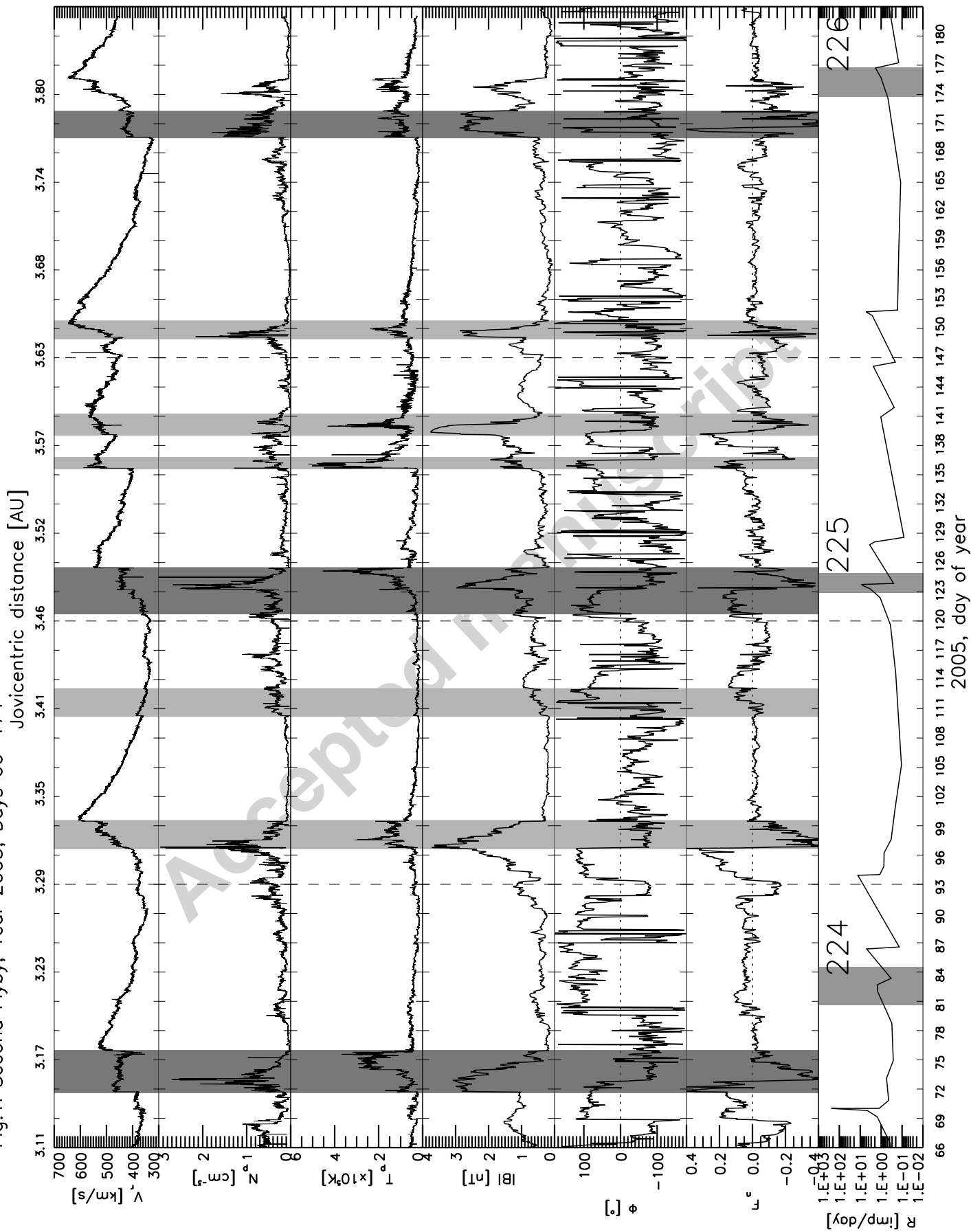
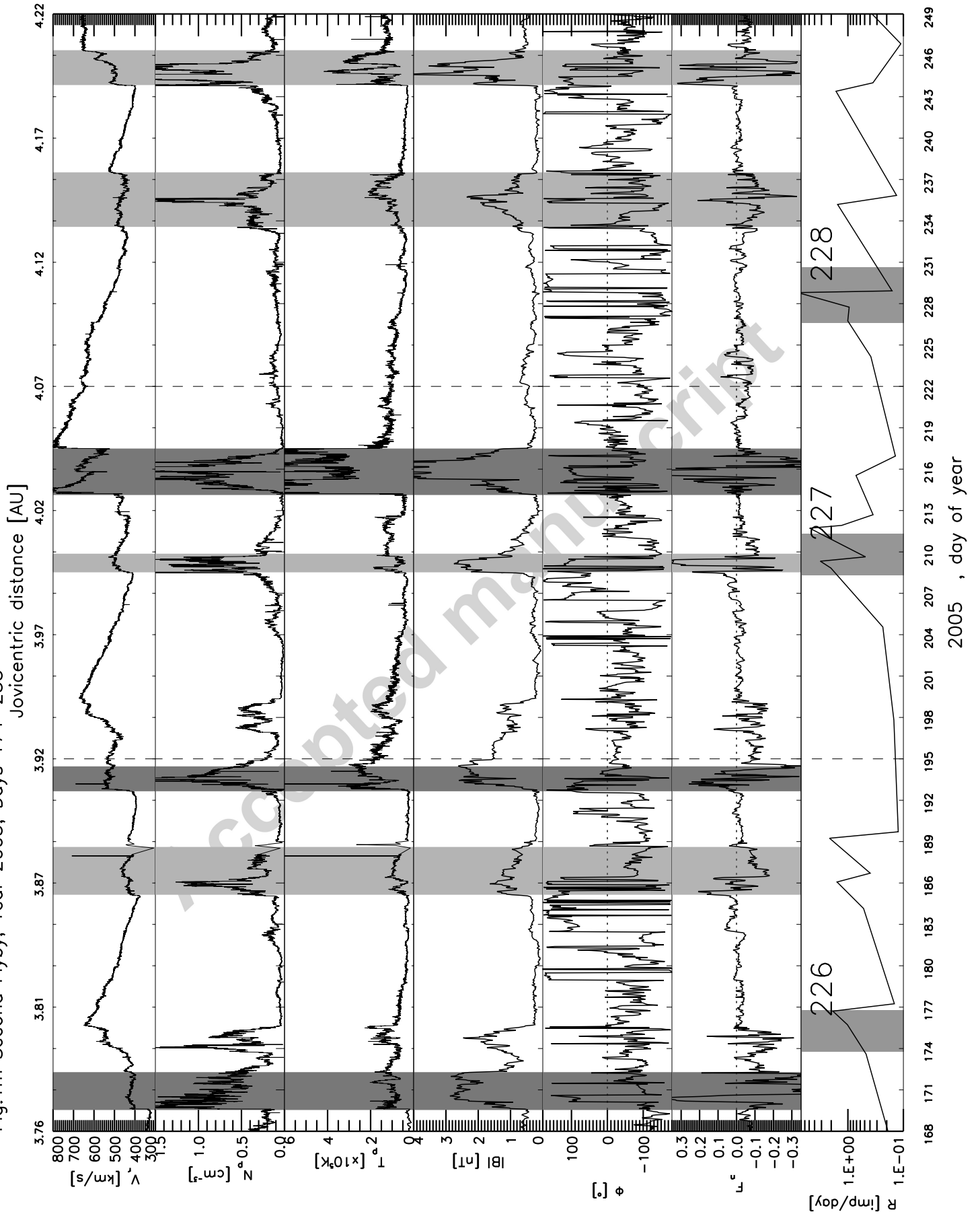


Fig.1m Second Flyby, Year 2005, Days 174–255



2005, day of year

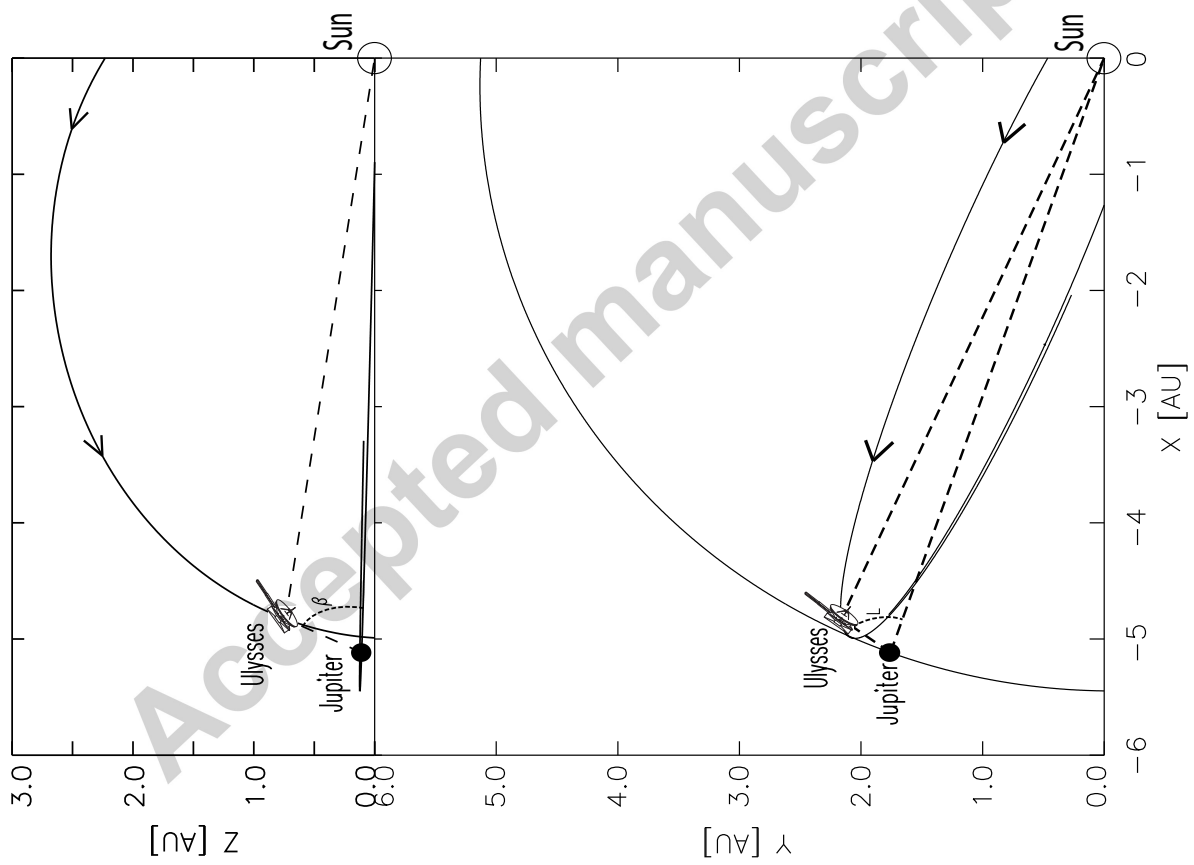
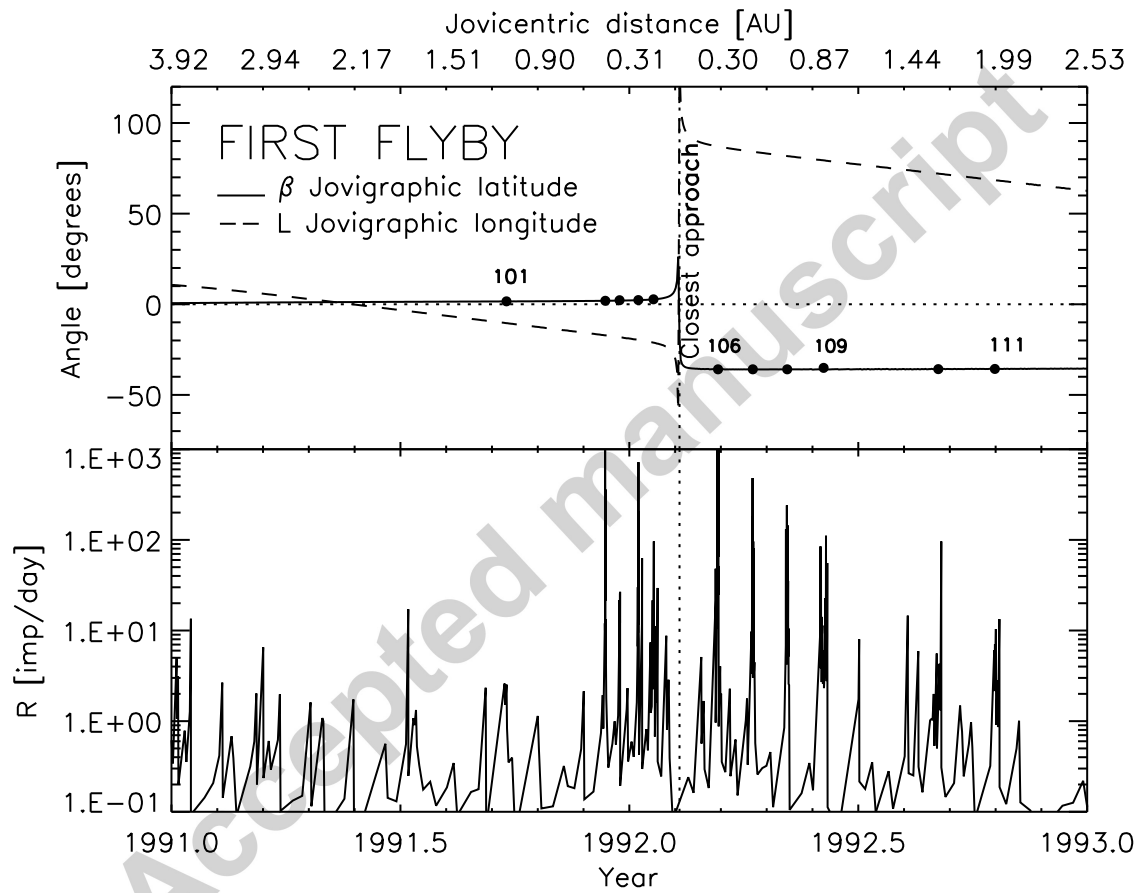
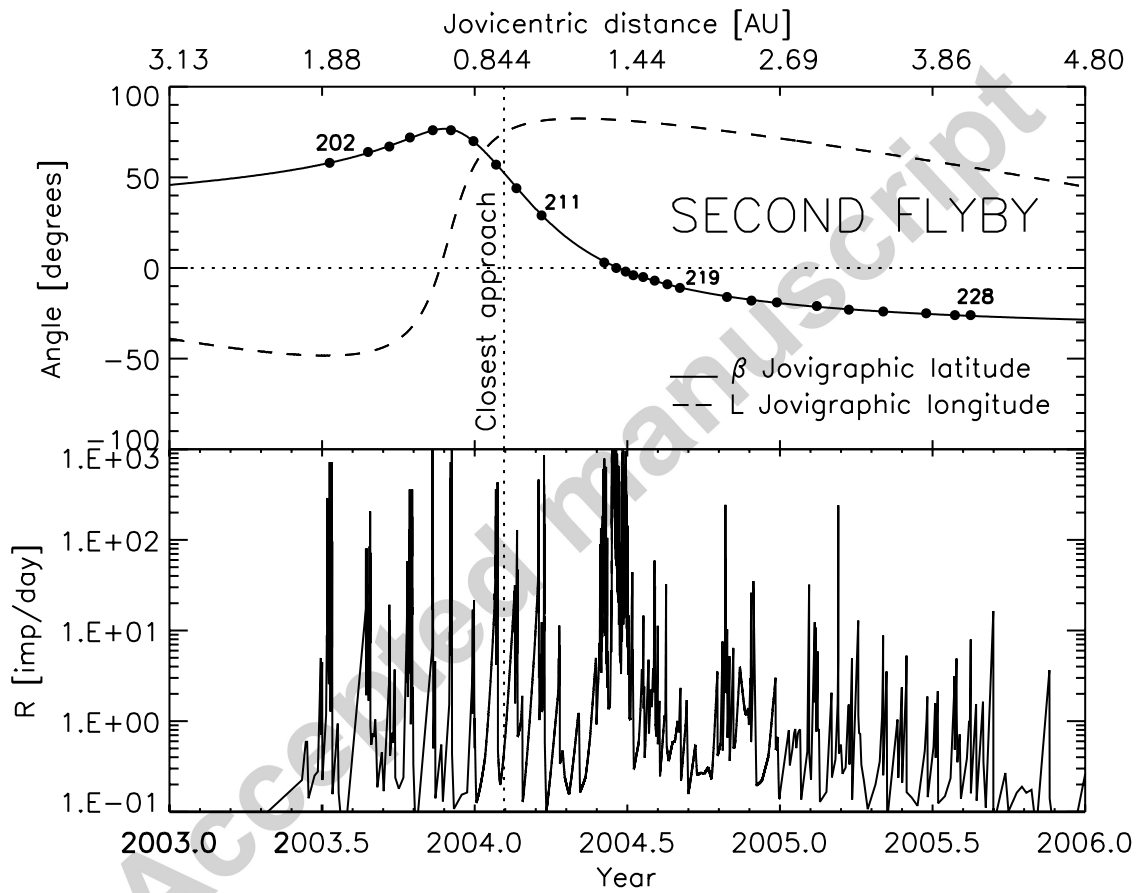
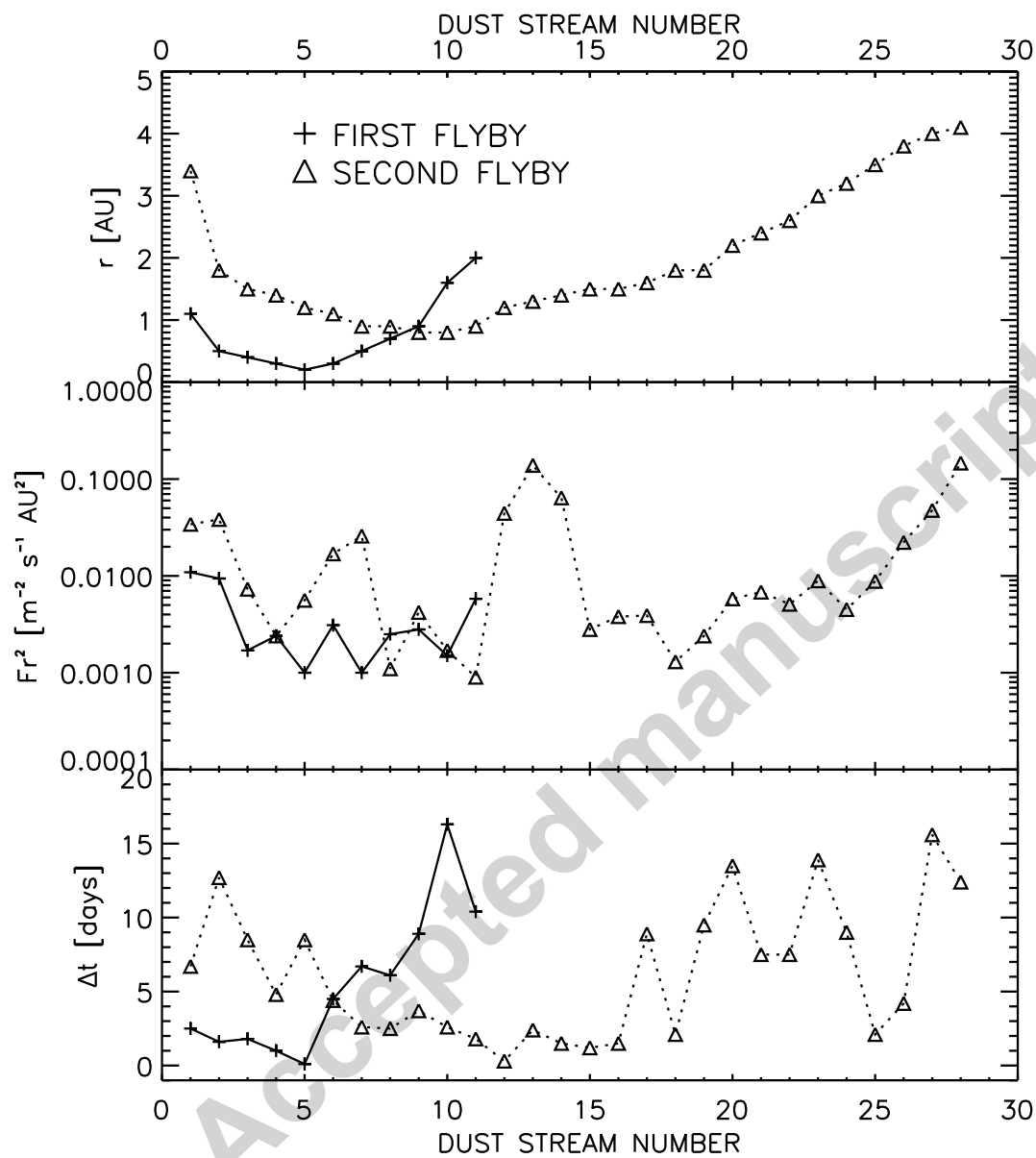
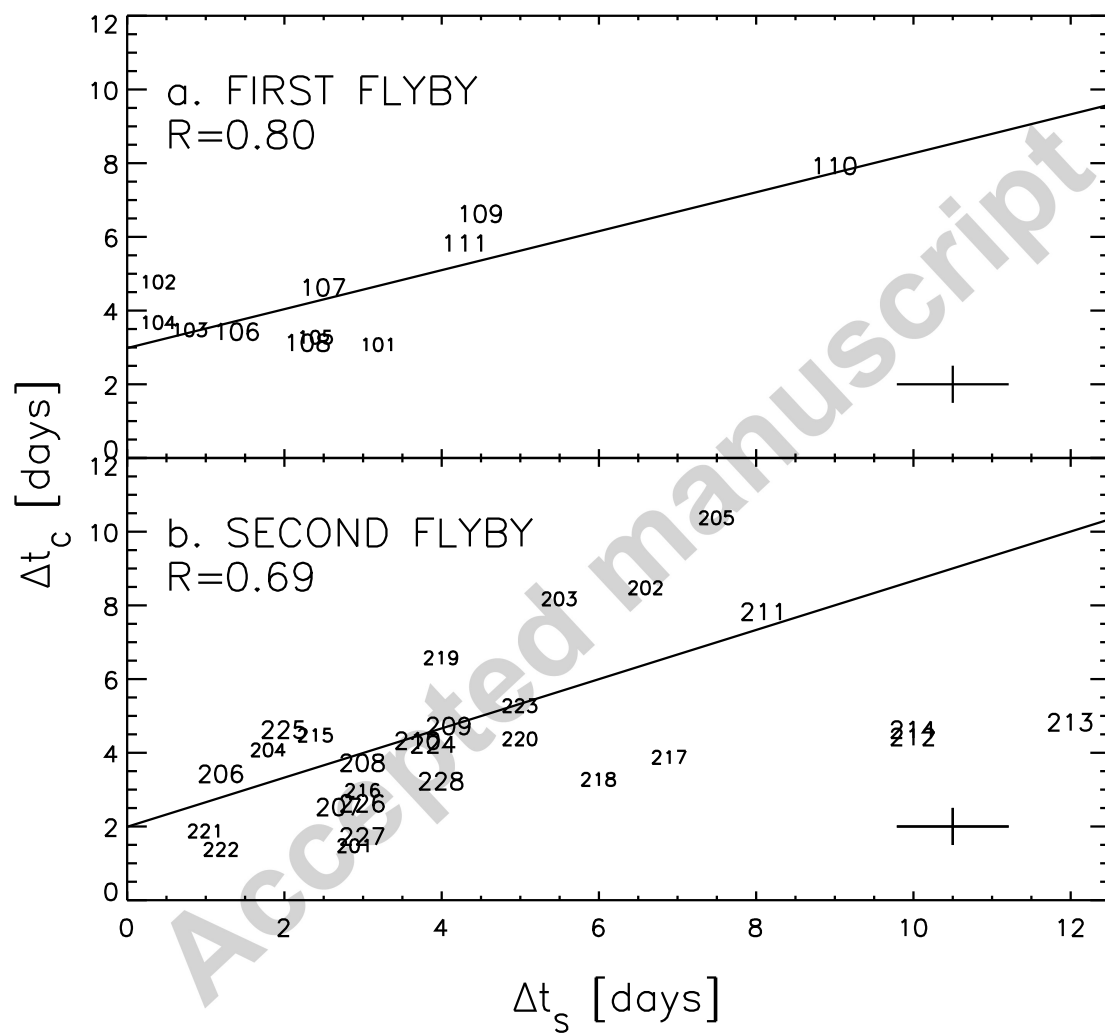


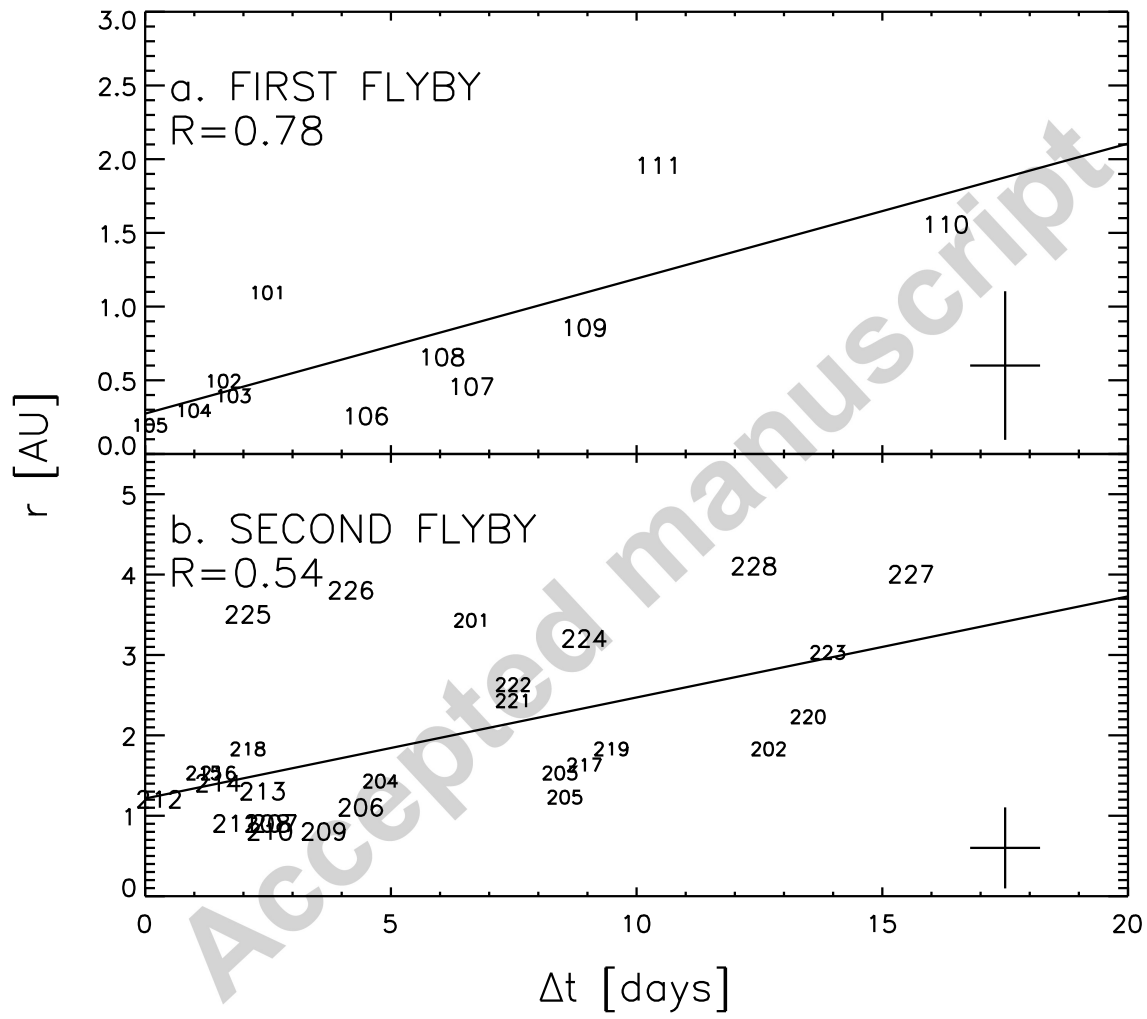
Figure 2

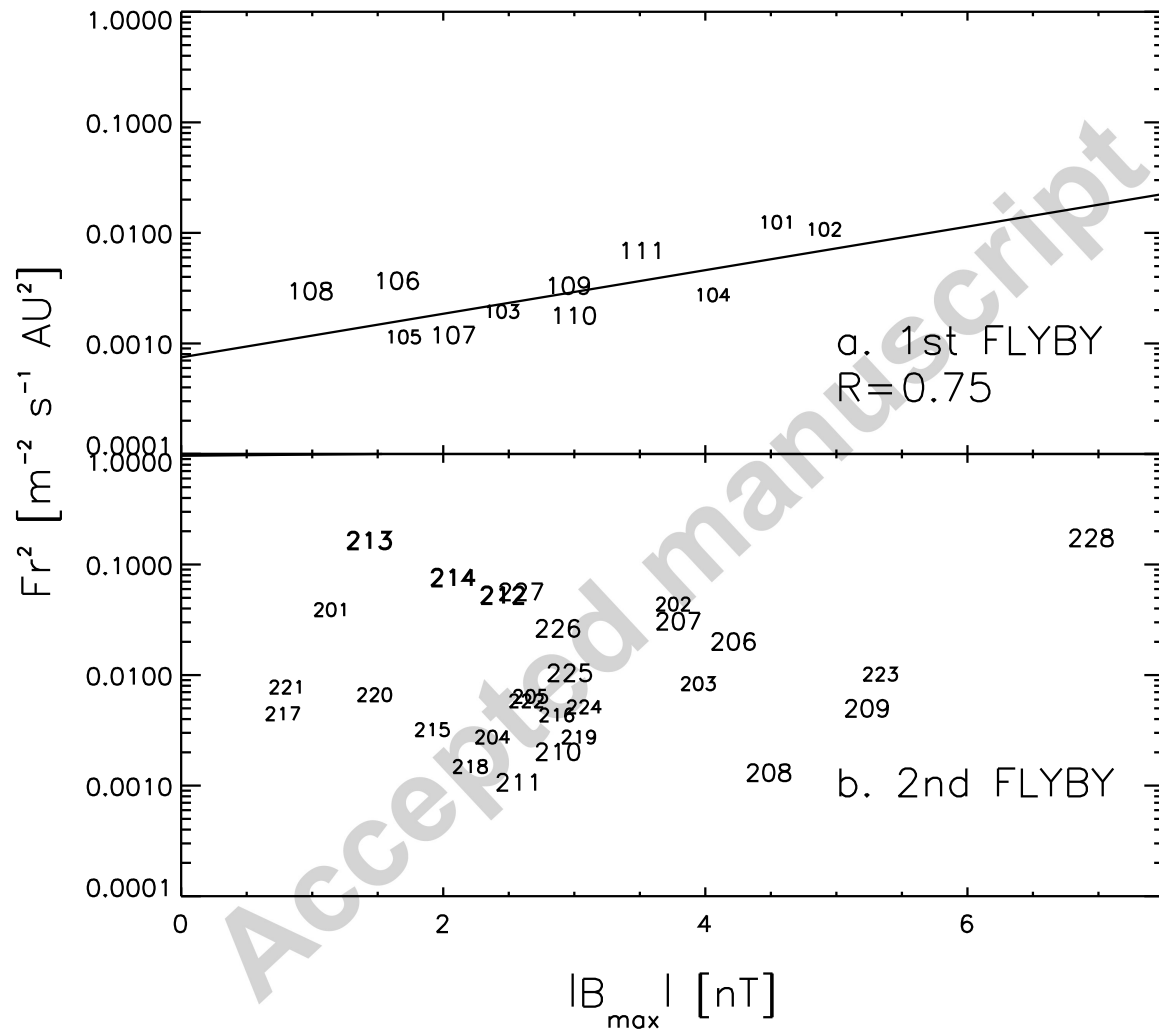












-So-called Jovian dust streams are strongly affected by the periodic variations of the solar wind.

-Dust streams' occurrence, intensity and duration are always linked to the solar wind structure.

-In summary, strong enough CIRs and CMEs are key in the detection of dust streams.

Accepted manuscript